THE ASTROPHYSICAL JOURNAL, 463:424–443, 1996 June 1

SOFT X-RAY PROPERTIES OF A COMPLETE SAMPLE OF RADIO-SELECTED BL LACERTAE OBJECTS

C. MEGAN URRY
Space Telescope Science Institute, 3700 San Martin Drive, Baltimore, MD 21218; cmu@stsci.edu
RITA M. SAMBRUNA[1]
Space Telescope Science Institute, 3700 San Martin Drive, Baltimore, MD 21218; sambruna@stsci.edu
D. M. WORRALL
Harvard-Smithsonian Center for Astrophysics, 60 Garden Street, Cambridge, MA 02138
R. I. KOLLGAARD AND ERIC D. FEIGELSON
Pennsylvania State University, Department of Astronomy and Astrophysics, University Park, PA 16802
ERIC S. PERLMAN
Goddard Space Flight Center, Code 668, Greenbelt, MD 20771
AND
JOHN T. STOCKE
Center for Astrophysics and Space Astronomy, Campus Box 389, University of Colorado, Boulder, CO 80309
Received 1995 May 31; accepted 1995 December 8

ABSTRACT

We report the soft X-ray properties of the complete 1 Jy sample of 34 radio-selected BL Lacertae objects (RBLs) as measured with the *ROSAT* Position Sensitive Proportional Counter. The 0.1–2.0 keV spectra of RBLs are generally well described by a single power-law model modified at low energies by absorption in our Galaxy. In a few brighter cases, either a convex or concave spectrum was detected. The distribution of the X-ray photon indices for the RBL sample is quite broad, $1 < \Gamma < 3$, with a measurable intrinsic dispersion. Comparing the *ROSAT* spectral index distributions of RBLs and other blazars, we find that RBLs have soft X-ray spectra similar to the X-ray–selected BL Lacertae objects (XBLs) of the EMSS complete sample, and both are steeper than more luminous (and more distant) strong emission-line blazars. Sorting the sources according to the ratio of their radio to X-ray fluxes into low-frequency peaked BL Lacertae objects (LBLs, which are mostly RBLs) and high-frequency peaked BL Lacertae objects (HBLs, which are mostly XBLs), the soft X-ray spectral index distributions for the two classes are statistically different, with LBLs being flatter than HBLs. The *ROSAT* spectra of RBLs are steeper than those obtained previously with the *Einstein Observatory* IPC at slightly higher energies, suggesting that for these objects a flatter (Compton) component emerges at or above ~ 1 keV. The *ROSAT* data confirm that RBLs are variable X-ray sources, on timescales as short as weeks or even hours. Spectral variability was detected for three of the six sources having more than two pointed observations. Two of these are flatter in the fainter state, in contrast to the trend seen in previous X-ray studies of BL Lac objects (mostly XBLs).

Subject headings: BL Lacertae objects: general — radio continuum: galaxies — X-rays: galaxies

1. INTRODUCTION

Blazars comprise both luminous quasars with strong, broad emission lines[2] and lower luminosity, weak-lined active galactic nuclei like BL Lac objects. Both types of blazars have smooth, rapidly variable, polarized continuum emission from radio through UV/X-ray wavelengths, and a number have been detected at gamma-ray energies. All have compact flat-spectrum radio cores, and many exhibit superluminal motion. These characteristics can be explained if the blazar continuum is interpreted as synchrotron and Compton-scattered emission from a relativistic jet oriented close to the line of sight (Urry & Padovani 1995).

While hundreds of flat-spectrum radio quasars have been discovered, relatively few BL Lac objects are known. There are only a handful of complete samples, most very small and available only recently. These include the radio-selected 1 Jy sample of 34 BL Lac objects (Stickel et al. 1991) and the X-ray–selected Extended Medium Sensitivity Survey (EMSS) sample of 23 BL Lacertae objects (Stocke et al. 1991; Morris et al. 1991; Perlman et al. 1996a). Other published samples of radio-selected and X-ray–selected BL Lac objects are considerably smaller (although larger *Einstein* Slew Survey and *ROSAT* samples of BL Lacertae objects will be available quite soon; Schachter et al. 1993; Perlman et al. 1996b; Wolter et al. 1996), and in sharp contrast to quasars, there are no sizable optically selected samples of BL Lac objects.

When BL Lac objects began to be discovered in X-ray surveys, it quickly became apparent that the continuum properties of X-ray–selected BL Lacertae objects are sys-

[1] Present address: NASA Goddard Space Flight Center, Code 666, Greenbelt, MD 20771; sambruna@attilla.gsfc.nasa.gov.

[2] Depending on how they were found, the strong emission line blazars are known variously as optically violently variable (OVV) quasars, flat-spectrum radio quasars (FSRQs), core-dominated quasars (CDQs), and highly polarized quasars (HPQs). In the latter case, only radio-loud HPQs are blazars; a few radio-quiet quasars also have highly polarized optical emission, and thus are HPQs, but their polarization is almost certainly caused by scattering rather than intrinsic emission processes.

tematically different (Ledden & O'Dell 1985; Stocke et al. 1985) from those of the "classical" BL Lac objects (Stein, O'Dell, & Strittmatter 1976), most of which were discovered as radio sources. While the definitions of radio-selected and X-ray–selected BL Lac objects are similar—flat-spectrum radio-loud active galaxies with featureless optical spectra (formally, for the 1 Jy sample, *rest* equivalent widths $W_\lambda \leq 5$ Å, optical magnitudes $V \leq 20$, and flat radio spectral index, $\alpha \leq 0.5$; for the EMSS, *observed* $W_\lambda \leq 5$ Å, Ca H/K breaks smaller than 25%, and no constraint on V or α)—the radio-selected BL Lacertae objects (RBLs) show more extreme optical variability, higher and more variable polarization, and less starlight fraction than X-ray–selected BL Lacertae objects (XBLs; Stocke et al. 1985; Jannuzi, Smith, & Eaton 1994). The X-ray luminosities of the two types (in current samples) are similar (Maraschi et al. 1986), but the RBLs have higher ratios of radio to ultraviolet or radio to X-ray flux densities than the XBLs (Ghisellini et al. 1986), more like those of strong emission line blazars (Maraschi et al. 1995; Sambruna, Maraschi, & Urry 1996). The extent to which selection effects are responsible is a matter of current debate (Giommi & Padovani 1994; Padovani & Giommi 1995).

The X-ray emission from BL Lac objects is a critical diagnostic of these differences in broadband continuum shape because the relative contributions of two high-energy components, synchrotron emission from the highest energy electrons and Compton-scattered emission from the lowest energy electrons, may be comparable at X-ray energies. Previous X-ray studies of BL Lacertae objects, which were limited to small and/or incomplete samples and sometimes depended on data with poor statistics, showed that the X-ray spectra of both RBLs and XBLs are generally steep above 2 keV, with photon indices $\Gamma \gtrsim 2$, possibly flattening at lower energies (Ohashi 1989; Barr et al. 1989; Sambruna et al. 1994a, b; Madejski & Schwartz 1989). The spectra of HPQs are generally flatter, $\Gamma \sim 1.5$ (Worrall & Wilkes 1990; Sambruna et al. 1994a, b). Few blazars show evidence of significant cold absorbing gas in excess of the line-of-sight Galactic column density (Madejski & Schwartz 1989; Worrall & Wilkes 1990), making them relatively bright in the soft X-ray band. The recent detections of several BL Lacertae objects by *EUVE* (Marshall, Fruscione, & Carone 1995; Fruscione 1996) is further evidence that these objects do not have significant intrinsic absorption.

With the *ROSAT* Position Sensitive Proportional Counter (PSPC) we can for the first time determine the X-ray properties of two sizable well-defined samples of RBLs and XBLs, namely the 1 Jy (Stickel et al. 1991) and EMSS (Stocke et al. 1991; Morris et al. 1991) samples. Extensive *ROSAT* observations of the EMSS XBLs have recently been published (Perlman et al. 1996a). In this paper we describe the X-ray properties of RBLs using *ROSAT* PSPC data for the 1 Jy sample. (Similar analyses for subsamples were done by Brunner et al. 1994 and Comastri, Molendi, & Ghisellini 1996.) The observations and data analysis are discussed in § 2 and the results in § 3. In § 4 we compare our results to the X-ray properties of EMSS XBLs and other blazar samples observed with the *ROSAT* PSPC, as well as to previous IPC observations of the same RBLs. Our conclusions are discussed in § 5. An Appendix describes our extrapolation of published 21 cm H I data to southern latitudes.

2. OBSERVATIONS AND DATA ANALYSIS

2.1. *ROSAT PSPC Observations of the 1 Jy Sample of Radio-Selected BL Lac Objects*

Thirty-two of the 34 RBLs in the 1 Jy sample were observed in pointed mode with the *ROSAT* PSPC. We included in our study all these data[3] plus some information from the *ROSAT* All-Sky Survey (Voges 1993). The complete 1 Jy sample of RBLs is listed in Table 1. Source redshifts (col. [2]) were taken from Stickel et al. (1991) and updated where possible from the recent literature. The line-of-sight column density of neutral gas in our Galaxy (col. [3]) was determined from the 21 cm survey of Stark et al. (1992) except where noted; specifically, the small-beam pointed measurements of Elvis, Lockman, & Wilkes (1989) were used where possible, and for two sources at declinations too far south for the Stark et al. survey (0537−441 and 2005−489) we estimated the column density by reflecting fits to N_H versus Galactic latitude in the north (see Appendix). The uncertainties in the absorption for the Stark et al. data are approximately $\Delta N_H \sim 1 \times 10^{20}$ cm^{-2} because of local fluctuations averaged out over the large 2° antenna beam; Elvis et al. estimated their uncertainties to be $\Delta N_H \sim 1 \times 10^{19}$ cm^{-2}; and for the values approximated by the fits in the Appendix, the uncertainties are $\Delta N_H \sim 3 \times 10^{20}$ cm^{-2}.

The log of the *ROSAT* observations (cols. [4]–[7] of Table 1) includes the number of the *ROSAT* image, the date(s) of the pointed observations, and the effective exposure times (after the removal of intervals of anomalous or variable background). The X-ray brightness is given in column (7) as the net source count rate in the extraction cell (see § 2.2) over the full energy range 0.1–2.4 keV. As is apparent from the table, the 1 Jy BL Lacertae objects were detected over nearly 3 orders of magnitude in X-ray flux. The three X-ray bright sources 0716+714, 1652+398 (Mrk 501), and 2005−489 were observed in long exposures, yielding more than 15,000 photons in each case. One BL Lac object, 1514−241 (AP Lib), was not detected and for four more (0454+844, 0814+425, 0820+225, and 0828+493), fewer than 100 counts were detected.

Crude spectral information is reported in column (8) via the hardness ratio, defined as in Bechtold et al. (1994): $R \equiv (H - S)/(H + S)$, where S equals the counts in PI channels 11–40 (0.11–0.40 keV), and H equals the counts in PI channels 41–245 (0.41–2.48 keV). There are published PSPC data for some 1 Jy BL Lacertae objects, as referenced in column (9). In particular, a second observation of 0454+844 in a brighter state (63 counts) than during our observation (30 counts) was described by Brunner et al. (1994), and in the following we use their spectral results.

Twenty of the 1 Jy BL Lac objects were also detected in scanning mode during the *ROSAT* All-Sky Survey (RASS; Voges 1993). We take as firm identifications those RASS sources within 25″ of the BL Lac position, as this is the attitude uncertainty for weak sources (*ROSAT* Mission Description, Appendix F). The RASS count rates (col. [10]) come from an automatic search performed by the *ROSAT* Guest Observer Facility for the AO4 proposal round (R. F. Petre 1995, private communication). The two objects for

[3] This research has made use of data obtained through the High Energy Astrophysics Science Archive Research Center Online Service, provided by the NASA-Goddard Space Flight Center.

1996ApJ...463..424U

TABLE 1

ROSAT PSPC OBSERVATIONS OF THE 1 JANSKY RADIO-SELECTED BL LACERTAE OBJECTS

Source	z	N_H^{Gal} ($\times 10^{20}$ cm^{-2})	ROR Number	Date of Observation	Exposure (s)	Count Rate[a] (counts s^{-1})	Hardness Ratio[b]	References	RASS Count Rate[c] (counts s^{-1})
0048−097[d]	...	3.52	RP70143300	93 Jul 4–15	8363	0.376 ± 0.008	0.31 ± 0.03	...	0.244 ± 0.027
0118−272	>0.557	1.53	RP70142700	93 Jul 10–11	2635	0.135 ± 0.008	−0.11 ± 0.06	...	0.086 ± 0.029
0138−097	>0.501	2.84	...	...	...	...	...	...	<0.03
0235+164	0.940	7.60[e]	RP70137985	93 Jul 21–Aug 1	14591	0.185 ± 0.004	0.98 ± 0.01	...	...
0426−380	>1.030	1.94	RP70142800	93 Feb 8	4048	0.045 ± 0.004	0.15 ± 0.09	...	0.075 ± 0.023
0454+844	0.112[f]	6.31	WP700140	91 Apr 4–6	3358	0.009 ± 0.005	...	1, 2	...
0537−441[d]	0.896	4.1[g]	WP700199	91 Apr 10–17	2598	0.352 ± 0.012	0.34 ± 0.03	2, 3	0.189 ± 0.028
0716+714[d]	>0.3[h]	3.7	WP700210	91 Mar 8–11	18143	0.888 ± 0.007	−0.02 ± 0.01	1, 2, 4	0.144 ± 0.023
0735+178	>0.424	4.54	RP700829	92 Oct 28–29	6684	0.082 ± 0.004	0.56 ± 0.04	2	0.115 ± 0.019
0814+425	0.258?	4.92	RP700830	92 Oct 6–16	6120	0.014 ± 0.002	0.90 ± 0.13	...	...
0820+225	0.951	4.20	RP700831	92 Oct 29–30	3728	0.016 ± 0.002	0.72 ± 0.18	...	...
0823+033	0.506	3.49	...	...	...	...	...	...	<0.03
0828+493	0.548	3.94	RP700832	92 Oct 3–4	4821	0.013 ± 0.002	0.85 ± 0.19	...	...
0851+202[i]	0.306	2.75[e]	WP700219	91 Apr 16	2822	0.268 ± 0.010	−0.01 ± 0.02	2	...
			RP700426	91 Nov 10–11	6785	0.584 ± 0.009	0.34 ± 0.04	2	...
0954+658	0.367	4.28	RP700042	91 Apr 17–25	6772	0.050 ± 0.003	0.98 ± 0.04	2, 5	0.044 ± 0.012
1144−379	1.048	8.67	RP70143400	93 Jul 7–8	7747	0.110 ± 0.004	0.85 ± 0.02	...	...
1147+245	...	2.03	RP700833	93 May 27–29	10942	0.022 ± 0.002	0.33 ± 0.09	...	...
1308+326	0.997	1.08	WP700216	91 Jun 23	7574	0.095 ± 0.004	−0.13 ± 0.05	2	0.060 ± 0.012
1418+546	0.152	1.30	WP150046	90 Jul 19	11516	0.216 ± 0.004	−0.10 ± 0.02	2	0.103 ± 0.019
1514−241[d]	0.049	8.80	RP70142900	93 Aug 17	2915	<0.006[j]	...	...	0.053 ± 0.013
1519−273[d]	...	8.90	RP70143000	93 Aug 17–18	2552	0.100 ± 0.007	0.95 ± 0.04	...	0.032 ± 0.010
1538+149	0.605	3.23	RP700834	93 Jan 28–30	7215	0.034 ± 0.002	0.75 ± 0.08	...	0.083 ± 0.025
1652+398[d]	0.033	1.73[e]	RP700130	91 Feb 25–26	6599	6.898 ± 0.033	−0.08 ± 0.001	2	4.666 ± 0.108
1749+096	0.320	9.61	RP700043	91 Mar 17	3963	0.078 ± 0.005	1.08 ± 0.05	5	...
			RP700043	92 Mar 28	4944	0.073 ± 0.004	1.05 ± 0.04	5	...
1749+701	0.770	4.01	RP700835	92 Nov 9	3702	0.078 ± 0.005	0.15 ± 0.07	1	0.083 ± 0.013
1803+784[d]	0.6797	4.02	RP700836	92 Jul 25–Dec 10	5602	0.103 ± 0.004	0.49 ± 0.04	1, 2	0.062 ± 0.013
			WP700497	92 Apr 7	6911	0.075 ± 0.003	0.71 ± 0.04	2	...
1807+698	0.051	4.94	WP700489	92 Apr 9	10461	0.115 ± 0.003	0.56 ± 0.03	2	0.206 ± 0.023
1823+568	0.664	4.20	RP700837	92 Jun 19–20	5900	0.130 ± 0.005	0.90 ± 0.02	...	0.105 ± 0.013
2005−489[d]	0.071	4.1[g]	WP700488	92 Apr 27	10487	2.960 ± 0.035	0.12 ± 0.01	2, 6	2.610 ± 0.093
			WP701057	92 Oct–Nov	11462	1.650 ± 0.012	0.01 ± 0.01	2, 6	...
2007+777	0.342	8.90	WP700498	91 Dec 11	4574	0.034 ± 0.003	1.39 ± 0.10	1	0.034 ± 0.009
			WP700498	92 May 17	4156	0.046 ± 0.004	1.18 ± 0.08	...	...
2131−021	0.557?	4.24	RP70143100	93 Nov 2–3	7748	0.018 ± 0.002	0.64 ± 0.13	...	...
2200+420[d]	0.069	20.15[e]	RP700838	92 Dec 22–23	2167	0.158 ± 0.009	1.01 ± 0.02	...	0.089 ± 0.015
2240−260	0.774	1.46	RP70143200	93 Nov 9	3656	0.048 ± 0.004	−0.16 ± 0.10	...	...
2254+074	0.190	5.39	RP70143500	93 Nov–Dec	1753	0.028 ± 0.005	0.70 ± 0.18	...	...
			RP70143500	94 Jun 3–4	11487	0.030 ± 0.005	0.79 ± 0.05	...	...

[a] Count rate in the spectral extraction cell (§ 2.2) over the full 0.1–2.4 keV range.
[b] Hardness ratio, R, defined in § 2.1.
[c] R. F. Petre 1995, private communication.
[d] Significantly variable between RASS and pointed observations.
[e] From Elvis et al. 1987.
[f] From Brunner et al. 1994.
[g] From Appendix.
[h] Wagner et al. 1993.
[i] Probably variable between RASS and pointed observations.
[j] 3 σ upper limit.

REFERENCES.—Brunner et al. 1994; (2) Comastri et al. 1995; (3) Treves et al. 1993; (4) Cappi et al. 1994; (5) Worrall et al. 1993; (6) Sambruna et al. 1995.

which pointed *ROSAT* PSPC observations were not performed, 0138−097 and 0823+033, were not detected in the All-Sky Survey so we have estimated crude upper limits of ~ 0.03 counts s^{-1} for their X-ray count rates based on the minimum observed count rates for objects with similar exposure times during the survey (i.e., at ecliptic latitudes less than $\sim 75°$). For roughly one-third of the 1 Jy BL Lac objects, substantial long-term variability, by up to a factor of 6, can be inferred from comparing the mean count rates of the RASS and pointed observations. The variability of the six objects observed at separate epochs in pointed mode (0851+202, 1749+096, 1803+784, 2005−489, 2007+777, and 2254+074) is discussed in § 3.4.

2.2. *Extraction of Source and Background Photons*

For most observations, source counts were extracted (using IRAF v.2.10.3) from a circle with radius 1′ centered on the target position; at 1′, the total counts are generally comparable to the background counts, as verified by analysis of the radial surface brightness profiles. For 0048−097, 0716+714, 0851+202 in its brighter state, 1652+398, and 2005−489, for which more than 3000 counts were detected, the radial profiles showed that a radius of 2′ was needed to collect all the soft photons and avoid the "ghost-image" problem (Briel et al. 1994). The background was evaluated in an annulus with inner radius 2′ and outer radius 4′ (3′ and 5′ for the brighter sources listed above), excluding $\lesssim 1'$ circles around other detected sources. The background light curves were examined carefully for flares or anomalous trends and data were time-filtered to exclude intervals of variable background. Data were then extracted over the full energy range 0.1–2.4 keV in 256 PI channels. To avoid the known problem of overestimation of errors upon rebinning, we set the parameter POISSERR = YES in the QPSPEC file (see *ROSAT* Status Report 103, 1994 September 6, accessible at http://heasarc.gsfc.nasa.gov/docs/rosat/status) The final background-subtracted data have signal-to-noise ratios in the range 6–140, with a median value ~ 14.

We note that no obvious serendipitous sources are present within 2′ of most BL Lacertae objects. The exceptions are 0954+658, 1538+149, 1749+096, 1749+701, 1823+568, and 2200+420, near each of which a few (1–3) faint sources were found at an intensity level 1% to 8% that of the target. A full description of the serendipitous sources in the PSPC fields of the 1 Jy RBLs can be found in the WGA catalog of *ROSAT* sources (White, Giommi, & Angelini 1994).

In the case of 0235+164, the radial profile shows an excess of ~ 60 soft counts (PI channels < 41, $E < 0.5$ keV) between 110 and 190 pixels (0.′9–1.′6), at a position angle of $\sim 280°$. It is not clear at present whether these photons are related to the target via the ghost-image effect or are a close, faint source. As a conservative choice, they were excluded from the analysis.

Some 1 Jy RBLs have nearby companions and/or appear to lie in optical clusters of galaxies, including 1514−241 and 2005−489 (Pesce, Falomo, & Treves 1994), and 3C 371, 1418+546, and 2254+074 (Fried, Stickel, & Kühr 1993). Several others are surrounded by an apparent excess of galaxies relative to the field, including 0851+202 and 2200+420 (Smith, O'Dea, & Baum 1995). The PSPC images show no evidence for diffuse X-ray emission around these objects or the other 1 Jy RBLs.

2.3. *Timing Analysis*

While X-ray variability was not the prime focus of our study, the low-background PSPC data allow a sensitive search for variability on short timescales. The detection of variability could also complicate our spectral analysis, so we searched for time variability in each BL Lac light curve applying Kolmogorov-Smirnov (K-S) and χ^2 tests. Both methods can be used to detect variability on timescales comparable to or shorter than the exposure times; depending on the source strength and the character of the variability, either method could be more sensitive. The satellite wobble introduces spurious variability on timescales of the wobble period, ~ 400 s, so all light curves were rebinned with $t_{\rm bin} = 400$ s, or more for count rates less than ~ 0.03 counts s^{-1}.

For three BL Lacertae objects (0235+164, 0716+714, and 1418+546), significant X-ray variability was detected (there is less than 1% chance according to a K-S test that the cumulative photon distribution is uniform). The X-ray intensity of 0235+164 increases by a factor of 1.7 in ~ 3 days, then decreases by a factor of 3.5 in 13 days. The flux from 1418+546 dims by 40% in ~ 3 days. The X-ray intensity of 0716+714 decreases by a factor of ~ 7 in 2 days, with associated spectral changes; a flare is also present, with an increase of $\sim 70\%$ in less than ~ 3 hr (Witzel et al. 1993; Cappi et al. 1994). This particular BL Lac object is known for its extremely rapid correlated variability at radio and optical wavelengths (Quirrenbach et al. 1989). In the remaining cases no significant variability was detected with either the K-S or χ^2 tests.

Rough estimates show that the K-S test is sensitive to slow trends with 5%–20% increases in the brighter sources (thousands of counts) or 50%–100% increases in the fainter sources (tens or hundreds of counts) at the $P = 99\%$ confidence level. The χ^2 test is sensitive to a factor of 2.7 (1.3) [1.1] flare for $N = 100$ (1000) [10,000] counts at the 3 σ confidence level, assuming a 10% flare duty cycle. The range of timescales sampled is limited on the short end by the spacecraft wobble and on the long end by the typical length of an observation (less than ~ 10 ks in most cases), so that with these data we were sensitive to only about one decade in temporal frequency. Thus, it is not surprising that, although BL Lac objects are noted for frequent, rapid X-ray variability, we find few examples of rapid variability among this sample. Longer timescale variations, determined from repeated observations of individual sources, are discussed in § 4.2.

2.4. *Spectral Analysis*

Source spectra were analyzed for 28 of the 1 Jy RBLs, for which 85 or more counts were detected. The 256 channel spectra were rebinned such that each new bin contains at least 20 counts (using the command GRPPHA within FTOOLS) so the square root of the number of counts in a bin is a reasonable approximation of the uncertainty. Channels 1–10 and 200–256, where the background is higher and the spectral response is poorly calibrated, were excluded, so the resulting spectra cover the approximate energy range 0.11–2.0 keV.

Spectral fitting was done using XSPEC (Version 8.5). Different instrument response matrices were used depending on the date of observation. For data taken in "high-gain" mode (before 1991 October 14), the 92mar11 matrix was used, while the 93jan12 response was adopted for "low-

gain" (after 1991 October 14) data, as recommended in The *ROSAT* Users' Handbook (Briel et al. 1994). Spectral models were convolved with the response matrix and compared to the data, with spectral parameters determined according to the usual χ^2 minimization technique.

Each pair of observations of 2007+777 and of 2254+074, neither of which showed a significant change in intensity or spectral shape, was co-added for the spectral analysis. Co-addition was not possible for the two observations of 1749+096, which were taken in different gain settings.

As a first, simple approximation the data were fitted with a single power-law model modified at low energies by absorption due to neutral gas in the Galaxy. The absorbing column was parameterized in terms of $N_{\rm H}$, the H I column density, with heavier elements fixed at solar abundance. Cross sections were taken from Morrison & McCammon (1983). For one set of fits $N_{\rm H}$ was fixed at the Galactic value (col. [3] in Table 1), which leads to the tightest constraint on the photon spectral index. For all but the faintest of the 28 sources, 0814+425, we also did fits with $N_{\rm H}$ free to vary.

For the brightest BL Lac objects, a spectral shape more complex than a single power law was indicated. We explored both a broken power-law model and a single power law plus absorption edge or notch for the individual objects and for the ensemble. The statistical significance of these more complex models with respect to the single power law was determined using the F-test, assuming as a threshold of minimal significance $P_F = 95\%$. Results of the spectral fitting are described in the next section.

3. *ROSAT* PSPC SPECTRAL RESULTS FOR THE 1 JANSKY BL LACERTAE SAMPLE

3.1. *Single Power-Law Fits*

Most of the PSPC spectra of RBLs were well fitted by a single power-law model with Galactic absorption. The fitted parameters (and 90% confidence uncertainties) for single power-law models are reported in Table 2. For the fixed-$N_{\rm H}$ fits, the table lists in columns (2)–(4) the photon index, Γ; the reduced chi-squared and number of degrees of freedom, χ^2_r(DOF); and the acceptance probability of the fit, P_{χ^2}. For the free-$N_{\rm H}$ fits, columns (5)–(8) give $N_{\rm H}$, Γ, χ^2_r(DOF), and P_{χ^2}. The unabsorbed flux density at 1 keV calculated from the fixed-$N_{\rm H}$ fit, $F_{1\ \rm keV}$, is listed in column (9). The errors quoted in Table 2 for Γ and $N_{\rm H}$ represent rectangles circumscribing the 90% confidence contours (Fig. 1) for two interesting parameters ($\Delta\chi^2 = 4.6$), and thus are conservative. The uncertainty on $F_{1\ \rm keV}$ is derived from the 90% confidence errors on the normalization of the best-fit power law.

The two-dimensional confidence contours for Γ and $N_{\rm H}$ for free-$N_{\rm H}$ fits are shown in Figure 1. Vertical lines mark the value of the Galactic column density and the associated 1 σ range for each source (*solid and dashed lines*, respectively). The fits with free $N_{\rm H}$ generally yield column densities consistent with the Galactic values and slopes in good agreement with those derived with fixed $N_{\rm H}$; i.e., these objects appear to lack significant amount of intrinsic cold absorbing gas. The utility of the free-$N_{\rm H}$ fits is, therefore, their conservative limits on the photon index in the face of uncertainty in the assumed value of the Galactic $N_{\rm H}$.

For the two sources that were detected but for which no detailed spectral analysis could be performed, we estimated the spectral shape using the hardness ratio (defined in § 2.1). For 0820+225 and 0828+493, hardness ratios of $R = 0.72 \pm 0.18$ and 0.85 ± 0.19 (Table 1), respectively, are similar to the values for radio-loud quasars and rather flatter than for radio-quiet quasars (Bechtold et al. 1994). For comparison, the RBLs with the flattest spectral index, 1823+568, which has $\Gamma = 1.15$, has $R = 0.9 \pm 0.02$, while the steepest source, 2005−489 ($\Gamma \sim 3$), has $R \sim 0$.

There are a few cases for which a single power law is either unacceptable or can be improved significantly with the addition of more parameters. These are discussed further in § 3.3, with the exception of the high-redshift BL Lac object 0235+164 ($z = 0.94$), for which the complex X-ray spectrum is likely caused by a known intervening absorption system at redshift $z = 0.524$ (Madejski 1994, and references therein). For this object, the fixed-$N_{\rm H}$ single-power-law fit to the PSPC spectrum is improved significantly ($\Delta\chi^2 = 119$ for 92 DOF, significant at 99.99% with an F-test) by adding a cold absorber at $z = 0.524$. The best-fit parameters, with $N_{\rm H}(z = 0)$ fixed at the Galactic value, are $N_{\rm H}(z = 0.524) = 4.3^{+1.7}_{-1.5} \times 10^{21}$ cm^{-2}, $\Gamma = 2.79^{+0.46}_{-0.41}$, and $F_{1\ \rm keV} = 1.6^{+0.3}_{-0.2}$ μJy (Table 2; see also Madejski et al. 1996a). In subsequent discussion of fixed-$N_{\rm H}$ fits we adopt these values of spectral index and flux density for 0235+164.

Other RBLs in the 1 Jy sample have intervening absorption systems and thus are potentially similar to 0235+164 (those in Table 1 with lower limits on redshift determined from absorption lines). Among them, only 0426−380 shows an X-ray absorption column density higher than Galactic (Table 2). This object is discussed in § 3.3.2.

3.2. *Distribution of PSPC Spectral Indices*

We now describe the distribution of spectral indices obtained from fixed-$N_{\rm H}$ single power-law fits to the PSPC data for the 1 Jy RBLs sample. In cases where these fits were unacceptable (0426−380, 0537−441, 0716+714, and 1652+398; $P_{\chi^2} \leq 2\%$), we used the photon indices determined from the free-$N_{\rm H}$ fits, which were acceptable. For objects with repeated observations, we include the multiple spectral measurements independently. Spectral parameters for 0454+844 were taken from Brunner et al. (1994). In total, 33 spectra of 29 objects were considered.

The distribution of the 33 photon indices is shown in Figure 2*a*. The mean value is $\langle\Gamma\rangle = 2.16$ with standard deviation 0.52, and the weighted average and dispersion are $\langle\Gamma\rangle = 2.77 \pm 0.01$. The latter is clearly dominated by the brightest sources, which happen to have steep spectra. The distribution in Figure 2*a* shows a large spread, ranging from $\Gamma \sim 1$ to $\Gamma \sim 3$. We therefore investigated whether this spread reflects an intrinsic spread in spectral indices or is due to measurement uncertainty in a sample of objects with a single spectral index.

First, we looked at the distribution of photon index residuals. We define the ith photon index residual as $(\Gamma_i - \langle\Gamma\rangle)/\sigma_i$, where Γ_i is the measured PSPC index for the ith object, σ_i is the 68% error derived from the contours in Figure 1 (averaged if asymmetric), and $\langle\Gamma\rangle$ is the simple average slope for the whole group. A residual thus represents the distance in individual σ of each measured photon index from the average index. For a homogeneous sample we expect the observed residual distribution to behave like a Gaussian with center at zero and unit dispersion. The observed distribution of residuals (Fig. 2*b*) has 11

TABLE 2

SINGLE POWER-LAW FITS TO THE PSPC SPECTRA OF THE 1 JANSKY RADIO-SELECTED BL LACERTAE OBJECTS

	N_H FIXED (GALACTIC VALUE)			N_H FREE				N_H FIXED
OBJECT	Γ	χ_r^2(DOF)	P_{χ^2}	N_H ($\times 10^{20}$ cm^{-2})	Γ	χ_r^2(DOF)	P_{χ^2}	Flux Density$_{1\ keV}$ (μJy)
0048−097.....	2.57 ± 0.07	0.82(92)	90%	$4.20^{+0.72}_{-0.68}$	2.79 ± 0.24	0.77(91)	94.5%	0.77 ± 0.05
0118−272.....	$2.20^{+0.20}_{-0.18}$	0.74(12)	72	$2.73^{+0.02}_{-1.43}$	$2.74^{+0.81}_{-0.68}$	0.53(11)	88.8	0.20 ± 0.04
0138−097.....	...	...	...	...	...	...	...	<0.06[a]
0235+164.....	...	...	...	$43.33^{+16.67}_{-15.33}$	$2.79^{+0.46}_{-0.41}$	0.71(90)	96[b]	$1.56^{+0.31}_{-0.20}$
0426−380.....	1.95 ± 0.27	2.93(6)	0.7	$5.28^{+3.82}_{-3.02}$	$3.20^{+1.35}_{-1.16}$	2.36(5)	3.8	0.09 ± 0.02
0454+844.....	...	...	...	...	...	...	...	0.03 ± 0.02[a]
0537−441.....	2.54 ± 0.13	1.56(35)	1.8	$2.54^{+0.99}_{-0.85}$	$2.04^{+0.34}_{-0.32}$	1.30(34)	12	0.78 ± 0.07
0716+714.....	3.02 ± 0.03	1.35(160)	0.23	$3.02^{+0.23}_{-0.24}$	2.77 ± 0.09	1.13(159)	12.2	1.17 ± 0.03
0735+178.....	$2.20^{+0.18}_{-0.20}$	1.43(21)	9.2	$5.05^{+1.81}_{-1.59}$	$2.34^{+0.53}_{-0.50}$	1.48(20)	7.6	0.22 ± 0.03
0814+425.....	$1.16^{+0.67}_{-0.90}$	0.11(2)	89	...	...	...	...	0.05 ± 0.01
0820+225.....	...	...	...	...	...	...	...	0.04 ± 0.006[a]
0823+033.....	...	...	...	...	...	...	...	<0.07[a]
0828+493.....	...	...	...	...	...	...	...	0.03 ± 0.005[a]
0851+202.....	2.16 ± 0.12	0.90(29)	62[c]	$3.58^{+1.28}_{-1.14}$	$2.42^{+0.42}_{-0.39}$	0.86(28)	68	0.44 ± 0.05
	2.60 ± 0.06	1.13(97)	17.3[d]	$2.48^{+0.44}_{-0.40}$	$2.50^{+0.18}_{-0.16}$	1.12(96)	19	0.93 ± 0.05
0954+658.....	$1.24^{+0.25}_{-0.29}$	1.09(13)	36.3	$9.20^{+30.91}_{-4.25}$	$1.96^{+1.96}_{-0.66}$	0.60(12)	84	0.16 ± 0.02
1144−379.....	$2.54^{+0.17}_{-0.19}$	0.81(34)	77	$9.48^{+2.50}_{-1.88}$	$2.67^{+0.39}_{-0.37}$	0.81(33)	76.4	0.41 ± 0.03
1147+245.....	$1.86^{+0.22}_{-0.24}$	1.54(9)	12.6	$3.0^{+2.7}_{-1.9}$	$2.18^{+0.85}_{-0.74}$	1.66(8)	10	0.045 ± 0.008
1308+326.....	1.95 ± 0.13	1.09(27)	33.7	$1.28^{+0.86}_{-0.67}$	$2.04^{+0.40}_{-0.27}$	1.11(26)	31	0.13 ± 0.02
1418+546.....	2.12 ± 0.06	1.28(71)	5.7	$1.35^{+0.42}_{-0.37}$	$2.14^{+0.20}_{-0.18}$	1.30(70)	4.8	0.30 ± 0.02
1514−241.....	...	...	...	...	...	...	...	<0.02[a]
1519−273.....	$2.03^{+0.38}_{-0.43}$	1.16(9)	31.6	$11.84^{+37.32}_{-6.09}$	$2.37^{+2.63}_{-0.93}$	1.22(8)	28	0.39 ± 0.06
1538+149.....	$1.66^{+0.26}_{-0.30}$	1.53(9)	13	$4.66^{+3.74}_{-3.00}$	$2.05^{+0.91}_{-0.90}$	1.60(8)	11.7	0.09 ± 0.02
1652+398.....	2.35 ± 0.01	1.99(178)	$\ll 10^{-3}$	2.43 ± 0.13	2.63 ± 0.05	1.00(177)	46.5	8.30 ± 0.13
1749+096.....	$1.77^{+0.38}_{-0.42}$	1.25(12)	24[e]	$33.48^{+0.16}_{-26.11}$	$3.33^{+3.20}_{-1.75}$	1.05(11)	40	0.13 ± 0.02
	$1.50^{+0.43}_{-0.48}$	0.31(13)	99[f]	$9.11^{+36.39}_{-5.35}$	$1.45^{+2.12}_{-0.75}$	0.33(12)	98	0.15 ± 0.02
1749+701.....	$2.77^{+0.23}_{-0.23}$	0.55(11)	87	$3.03^{+2.20}_{-1.71}$	$2.44^{+0.77}_{-0.66}$	0.50(10)	89	0.15 ± 0.03
1803+784.....	$1.74^{+0.18}_{-0.21}$	1.37(20)	12[g]	$4.49^{+1.87}_{-1.62}$	$1.86^{+0.50}_{-0.48}$	1.43(19)	10	0.23 ± 0.02
	2.27 ± 0.16	1.18(23)	24[h]	$4.52^{+1.53}_{-1.37}$	$2.42^{+0.46}_{-0.44}$	1.21(22)	22.3	0.26 ± 0.03
1807+698.....	2.28 ± 0.14	1.44(47)	2.5	$3.19^{+0.96}_{-0.87}$	1.81 ± 0.30	1.18(46)	18.8	0.32 ± 0.02
1823+568.....	$1.15^{+0.18}_{-0.19}$	0.85(31)	71	$5.92^{+2.90}_{-1.87}$	$1.44^{+0.39}_{-0.37}$	0.75(30)	84	0.42 ± 0.03
2005−489.....	2.90 ± 0.02	1.18(174)	5.4[i]	4.13 ± 0.19	2.94 ± 0.06	1.17(173)	5.9	5.00 ± 0.09
	3.07 ± 0.03	1.06(161)	30[j]	$3.53^{+0.23}_{-0.22}$	2.90 ± 0.09	0.95(160)	66.2	2.69 ± 0.07
2007+777.....	$1.66^{+0.37}_{-0.40}$	0.60(16)	90[k]	$9.85^{+22.95}_{-4.78}$	$1.75^{+0.45}_{-0.67}$	0.62/15	86.4	0.17 ± 0.02
2131−021.....	$2.05^{+0.41}_{-0.52}$	0.41(4)	80	$3.51^{+5.12}_{-3.24}$	$1.86^{+1.27}_{-1.18}$	0.5(3)	68	0.05 ± 0.01
2200+420.....	$1.94^{+0.46}_{-0.47}$	1.12(13)	33	$37.0^{+0.76}_{-27.2}$	$2.92^{+3.08}_{-1.84}$	1.13(12)	33	0.88(<1.0)
2240−260.....	$2.15^{+0.33}_{-0.31}$	0.84(5)	52	0.78(<3.0)	$1.79^{+0.12}_{-0.69}$	0.87(4)	48	0.07 ± 0.03
2254+074.....	$2.12^{+0.22}_{-0.24}$	1.36(15)	16	$8.80^{+3.4}_{-2.6}$	$2.89^{+0.63}_{-0.60}$	0.84(14)	63	0.09 ± 0.01

[a] Derived assuming an absorbed (N_H = Galactic N_H; see Table 1) power-law spectrum with $\Gamma = 2.2$ (see text).
[b] Fit with $N_H(z = 0)$ fixed at Galactic and a cold absorber at $z = 0.524$ (see text).
[c] Observation of 1991 April 16.
[d] Observation of 1991 November 10.
[e] Observation of 1991 March 17.
[f] Observation of 1992 March 28.
[g] Observation of 1992 April 7.
[h] Observation of 1992 July–December.
[i] Observation of 1992 April 27.
[j] Observation of 1992 October–November.
[k] Combined observations of 1991 December–1992 May.

residuals at $\gtrsim |3\ \sigma|$ from the expected Gaussian (*solid line*), while fewer than 1 would be expected. The total deviation from the mean (χ_T^2, defined as the sum of the square of the residuals) is 3900 for 32 degrees of freedom ($P_{\chi^2} \ll 10^{-3}$). The spectra of seven objects (0048−097, 0716+714, 0851+202 in high state, 1652+398, 1144−379, 1749+701, and 2005−489 in both states) are $\gtrsim +3\ \sigma$ steeper than the average for the total group ("steep tail"), while three objects (0954+658, 1803+784, and 1823+568) have spectra $\lesssim -3\ \sigma$ flatter than the average. Thus, it appears that the distribution of spectral indices is intrinsically broad. If the steep and flat spectra are removed, the distribution does behave like a Gaussian ($\chi_T^2 = 29$ for 21 DOFs, $P_{\chi^2} \sim 10\%$), as shown in Figure 2*c*.

To determine the intrinsic spread in spectral slopes quantitatively, we used a maximum likelihood test, which assumes that the intrinsic distribution of the photon indices is a Gaussian with center Γ_p and dispersion σ_p (Worrall

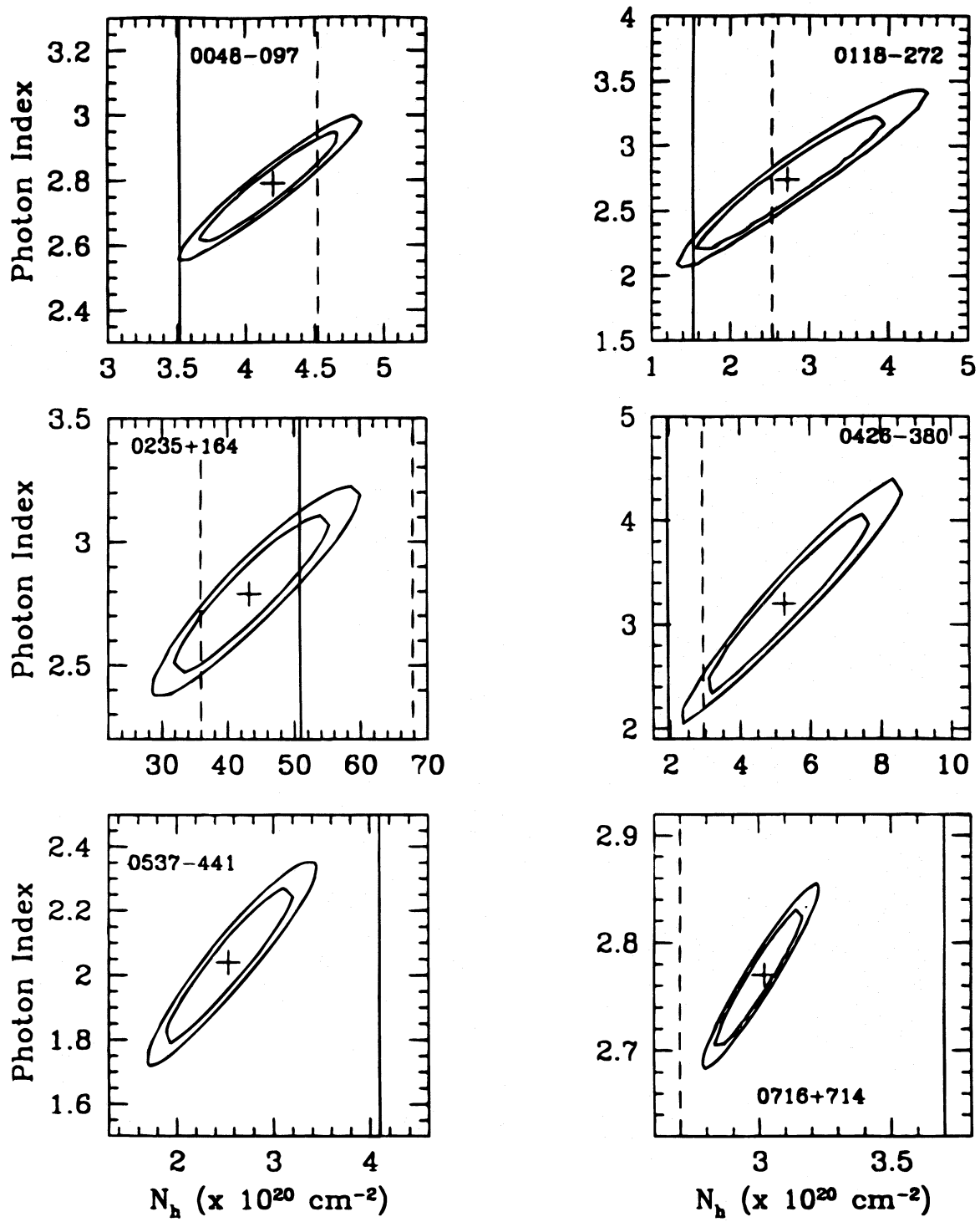

FIG. 1*a*

FIG. 1.—X-ray spectral fits for the complete 1 Jy sample of radio-selected BL Lac objects. Each plot shows the 68% (*smaller*) and 90% (*larger*) confidence contours in photon index (Γ) and column density of neutral absorbing gas along the line of sight (N_H) for free-N_H fits to the PSPC data. Vertical lines show the best estimate (*solid line*) and 1 σ uncertainty (*dashed line*) in line-of-sight Galactic N_H from 21 cm measurements (except for 0235+164, for which the quoted interval refers to the absorber at $z = 0.524$); most of the X-ray spectra are consistent with no absorption intrinsic to the BL Lac object.

1989). The derived 90% confidence contour for Γ_p and σ_p (Fig. 3, *solid line*) for the full RBL sample is clearly inconsistent with zero dispersion in spectral index, while when the spectra of the steep and flat tails are removed (*dotted line*), zero dispersion is (of course) allowed.

Because the 1 Jy sample includes RBLs out to redshift $z \sim 1$, the intrinsic spread in spectral slopes could be caused by a dependence of photon index on redshift, either because of a *K*-correction or spectral evolution. For example, the *ROSAT* PSPC spectral indices of optically selected quasars flatten with increasing distance, suggesting the presence of a flat component in the spectrum at higher energies (Brunner et al. 1993). However, no significant trend or correlation of PSPC slope with redshift is seen for the 1 Jy RBLs (Fig. 4).

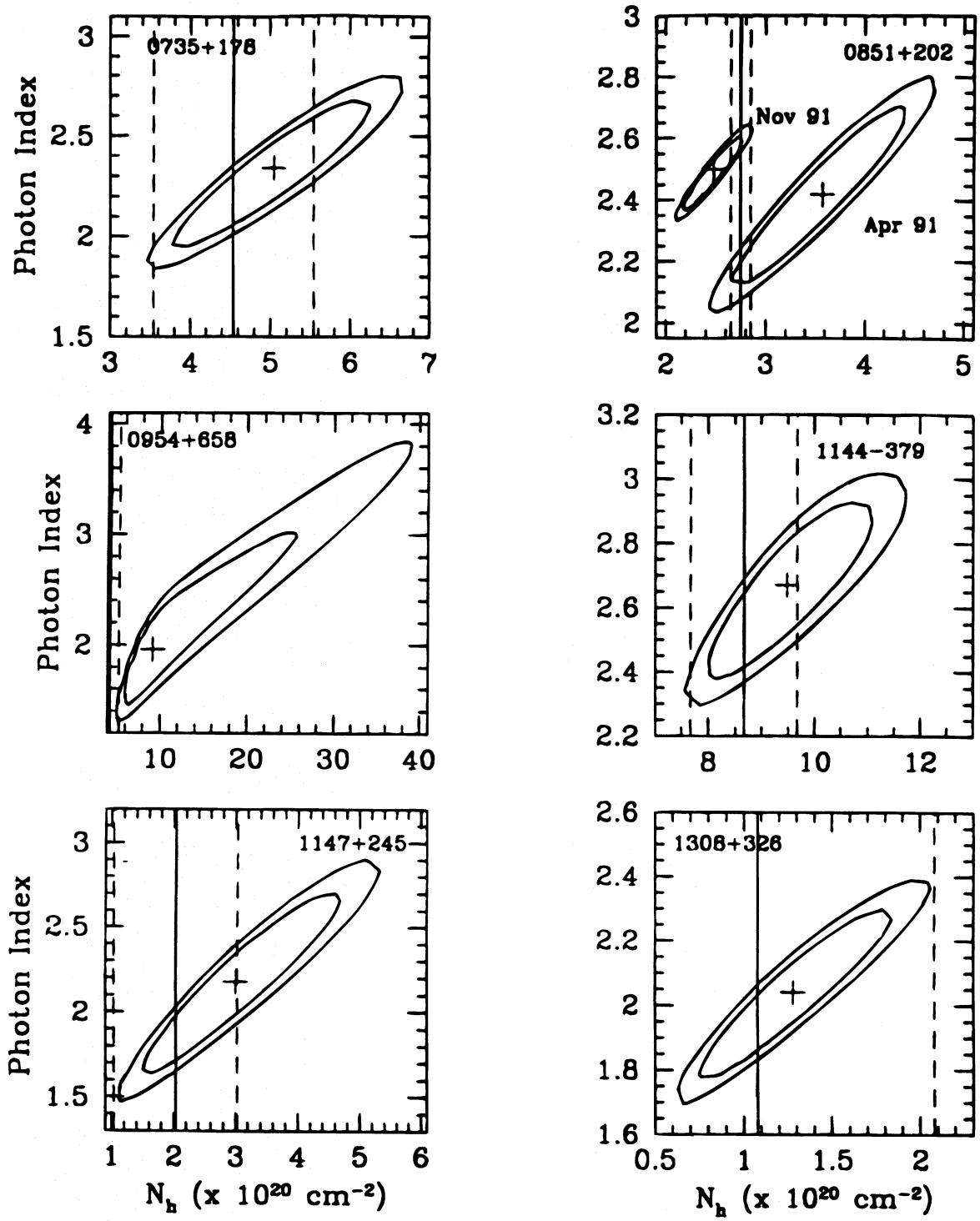

FIG. 1*b*

3.3. *More Complex Spectral Fits*

For a few of the brightest sources, the PSPC spectra are not well fitted by a single power law with N_H fixed at the Galactic value. Here we discuss more complex spectral models, including both broken power laws and simple power laws with discrete absorption in excess of the Galactic absorption (as might be caused by a highly ionized absorber).

The broken power-law model can be used to describe either convex (steepening with increasing energy) or concave (flattening with increasing energy) spectra. The free parameters are the break energy, E_0, and the two photon indices, Γ_1 and Γ_2, which describe the power-law spectral shape below and above the break, respectively. To minimize the number of free parameters, we fixed N_H at the Galactic value for these models. Note that convex (concave) spectra at the low resolution of the PSPC can often be described equally well by free-N_H single power-law models with the fitted N_H larger (smaller) than the Galactic value and by fixed-N_H broken power-law models.

We also considered single power-law models with discrete absorption, either an edge or a line (notch), in addition

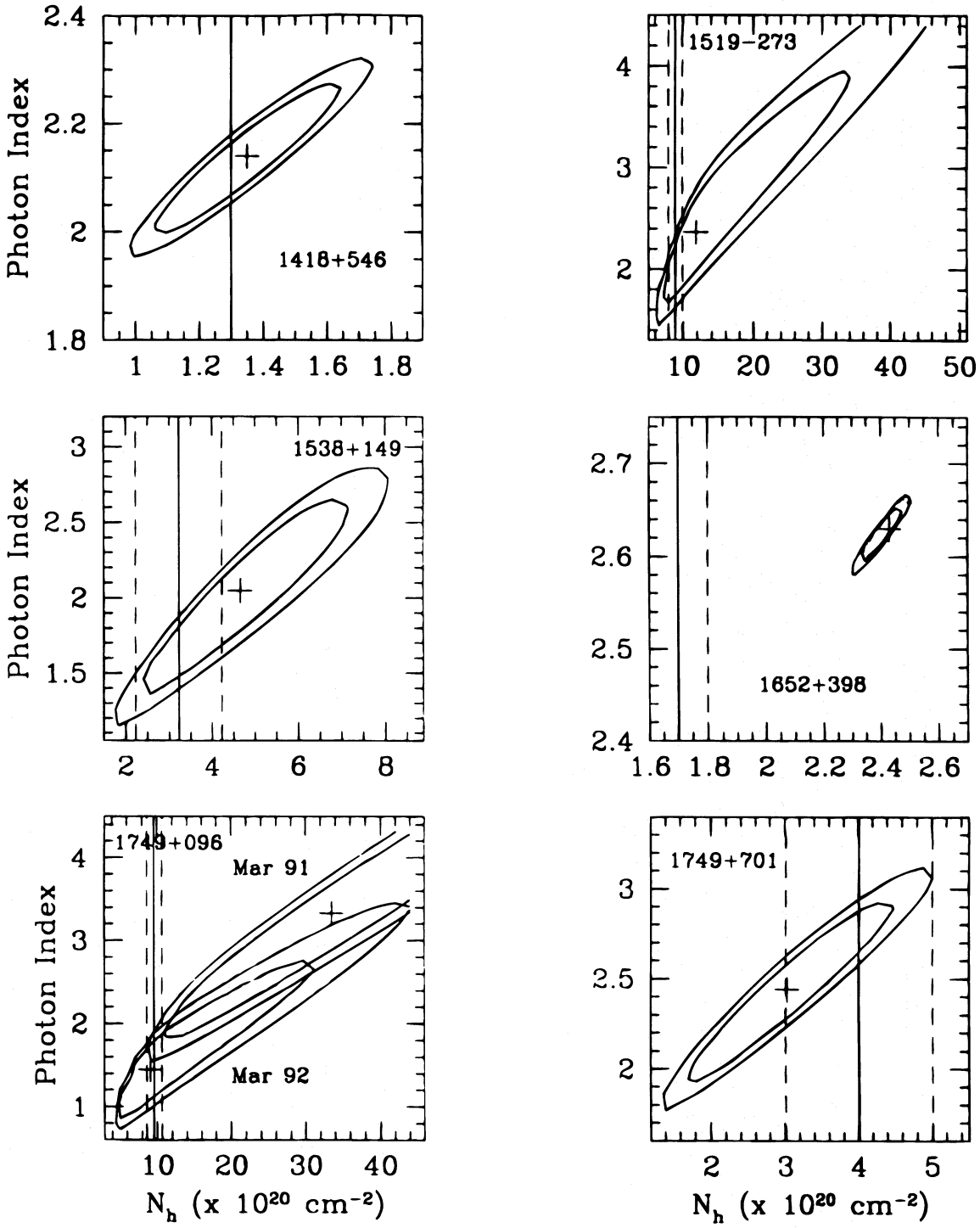

FIG. 1*c*

to fixed Galactic absorption. These models were motivated by the detection of such features in higher resolution X-ray spectra of the brighter BL Lac objects (Canizares & Kruper 1984; Madejski et al. 1991), most recently with BBXRT and *ASCA* (Madejski et al. 1996b; Tashiro et al. 1994). These absorption features have been interpreted as either edges or resonance absorption lines due to highly ionized oxygen. Here we considered a possible oxygen resonant line at $E_{\rm rest} = 0.654$ keV and single edges of ionized oxygen occurring between $E_{\rm rest} = 0.57$ keV (O II) and $E_{\rm rest} = 0.87$ keV (O VIII). The PSPC data are not very sensitive to the precise energy or form of the absorption because of the instrument's limited spectral resolution; however, because the PSPC is sensitive to much lower energies than the *Einstein* Solid State Spectrometer (SSS), *ASCA*, or BBXRT, it can in principal provide good limits on the strength of oxygen absorption. Simulations suggest that, providing the PSPC response matrix is known sufficiently well, a feature of the strength implied by the SSS or other higher resolution X-ray data should be detectable in our PSPC data for the brighter sources.

The broken power-law and discrete-absorption models were fitted to the few individual spectra for which the simple fixed-$N_{\rm H}$ power laws gave poor fits and were also applied

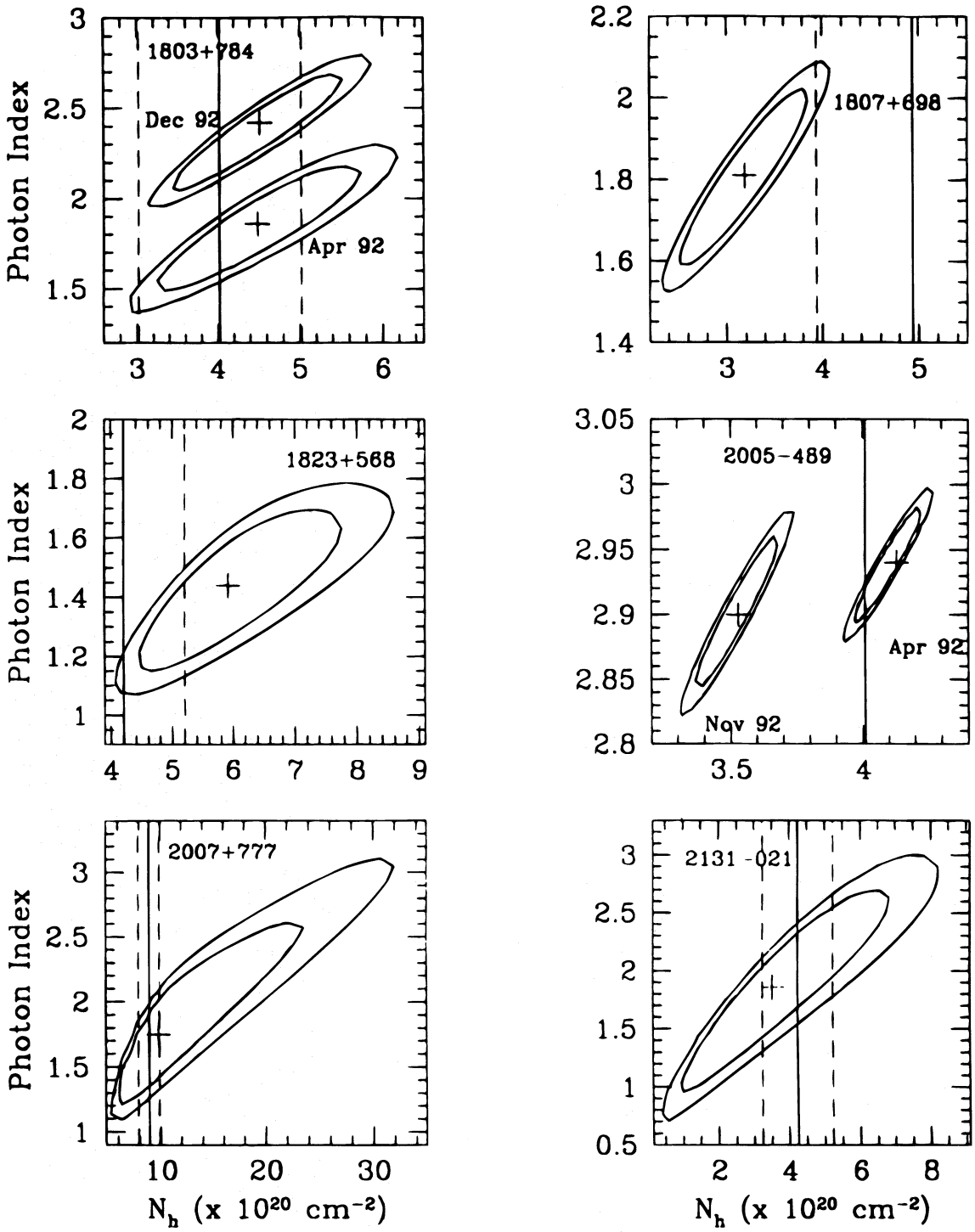

FIG. 1*d*

collectively to the ensemble of weaker sources. The following sections describe the results.

3.3.1. *1652+398* (Mrk 501)

The PSPC spectrum of the bright source 1652+398 (Mrk 501), for which a single power-law model with fixed N_H is clearly unacceptable ($P_{\chi^2} \ll 10^{-3}$), is shown in Figure 5. There is a systematic deficit of photons below ~ 0.2 keV, as is apparent from the residuals to a single power-law fit. The fit with free absorption is acceptable (and significant at more than 99% confidence according to an F-test); the fitted N_H is higher than the Galactic value and the spectral slope steeper than when the absorption is fixed, which is typical for a convex (downward curved) X-ray spectrum. A broken power-law model fits the PSPC spectrum of 1652+398 equally well and is also a significant improvement over a single power law plus Galactic N_H ($P_F >$ 99.9%). The best-fit parameters of this model are photon indices $\Gamma_1 = 1.32^{+0.38}_{-0.40}$ and $\Gamma_2 = 2.58 \pm 0.07$, and break energy $E_0 = 0.305^{+0.047}_{-0.027}$ keV, with $\chi^2_r = 1.0(176)$.

Previous observations of 1652+398 with the *EXOSAT* satellite in the energy range 0.1–10 keV also indicated a convex X-ray continuum, with a steepening of $\Delta\Gamma \sim 0.4$ above 3 keV (Sambruna et al. 1994a, b). The higher

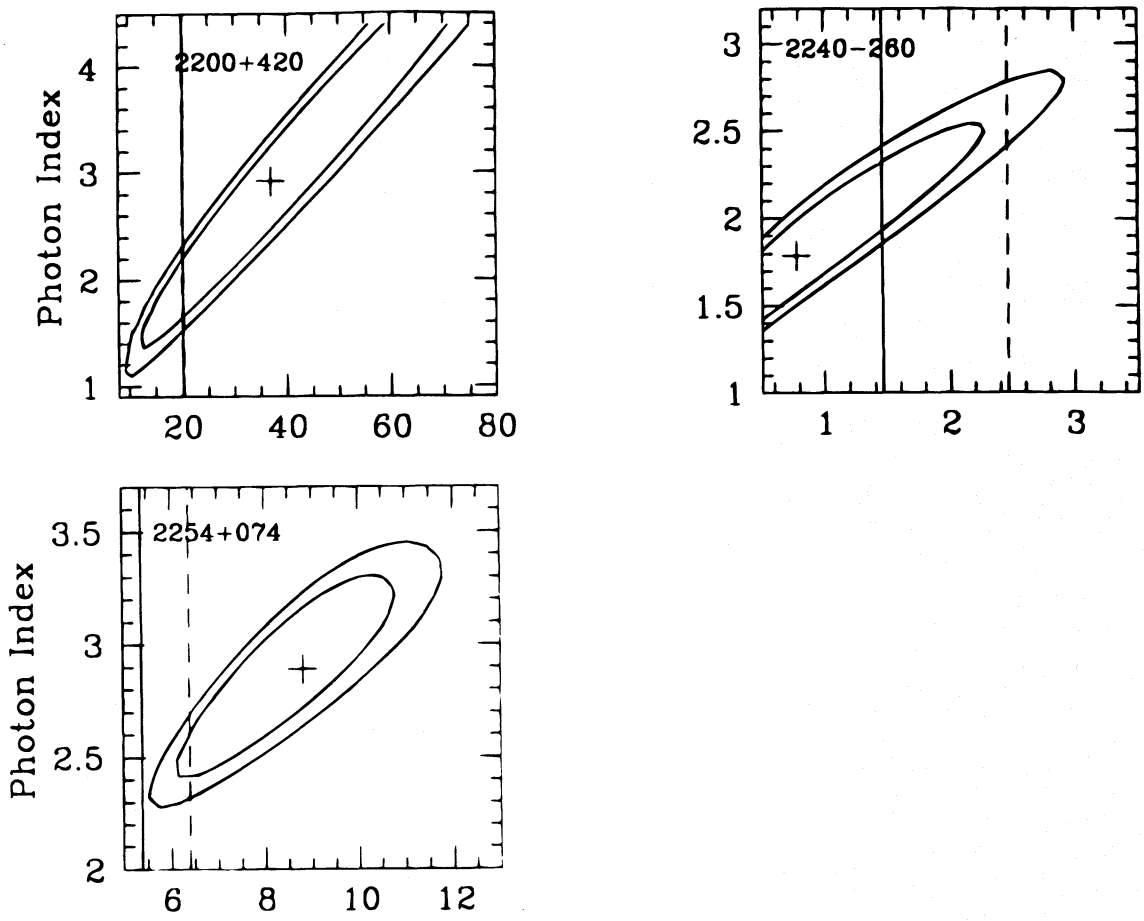

FIG. 1*e*

resolution *Einstein Observatory* SSS spectra of 1652+398 were consistent with the presence of oxygen absorption edge/line at $E_{\rm rest} \sim 0.56$ keV (Urry, Mushotzky, & Holt 1986; Madejski et al. 1991). The presence of a similar absorption feature could also cause the convexity observed in the *EXOSAT* spectrum, because of the lack of sensitivity of the latter experiment below ~1 keV.

In our PSPC data for 1652+398 there is no evidence of this kind of narrow absorption feature. We estimate an upper limit to the covering fraction, for line energy $E = 0.56$ keV and width $\Delta E = 0.1$ keV, of $f < 0.01$.

3.3.2. *0426−380, 0537−441, 0716+714, and 1807+698*

The fits with a single power-law model were unacceptable for four other objects in our sample. As mentioned in § 3.1, the *ROSAT* spectrum of 0426−380 is better fitted with a power law plus free $N_{\rm H}$ higher than the Galactic value (Table 2); however, the improvement of the fit with respect to the power law plus Galactic $N_{\rm H}$ is not significant and the fit is still relatively poor. Adding a cold absorber at $z = 1.03$, the redshift of a likely absorption system, to the fixed-$N_{\rm H}$ model yields an equally good fit, with fitted parameters $N_{\rm H}(z = 1.03) \sim 1.9 \times 10^{21}$ cm^{-2}, $\Gamma \sim 3.2$, $F_{1\ \rm keV} \sim 0.08$ μJy, steeper than the fixed-$N_{\rm H}$ fit. A broken power-law model also gives a good fit but with less obvious physical meaning. Higher quality X-ray data, as well as high-resolution optical spectroscopy, are necessary to confirm and measure possible intervening absorption systems in 0426−380. With the added absorption at $z = 1.03$, the X-ray spectral index becomes highly uncertain, so we refer to the fixed-$N_{\rm H}$ fits in subsequent discussion.

In the cases of 0537−441, 0716+714, and 1807+698 (3C 371), the fits with free $N_{\rm H}$ are significantly better than the fits with Galactic $N_{\rm H}$ at $\gtrsim$98% (0537−441) and >99% (0716+714 and 1807+698) confidence according to an *F*-test. The fitted column densities are lower than the Galactic values and the photon indices steeper than those determined from the fits with fixed absorption, which could indicate either a concave spectrum or the presence of an unresolved absorption feature at energies in the middle of the PSPC range (~0.5 keV).

For 0537−441 the fit with a broken power-law model is not better than the fit with the single power law and fixed $N_{\rm H}$. The model with a power law plus Galactic absorption plus absorption edge yields a significant improvement ($\Delta\chi^2 = 12.17$ for 33 DOF, ~95% significant from the *F*-test), with edge energy $E_{\rm e} \sim 0.3$ keV and optical depth $\tau_{\rm e} \sim 2$. However, the best-fit edge energy is suspiciously close to the edge of carbon, which is the primary constituent of the instrument entrance window. The still poorly calibrated gain shifts of the PSPC can create spurious deep ($\tau \sim 2$) absorption features (see Sambruna et al. 1995 for a simulation of this effect).

For 0716+714 the fit with a broken power-law model yields a significant improvement with respect to the single power-law model ($\Delta\chi^2 = 41$ for 158 DOFs, more than 99% according to the *F*-test), with a flattening of $\Delta\Gamma \sim 0.5$ above 0.5 keV, in agreement with Cappi et al. (1994). An equally

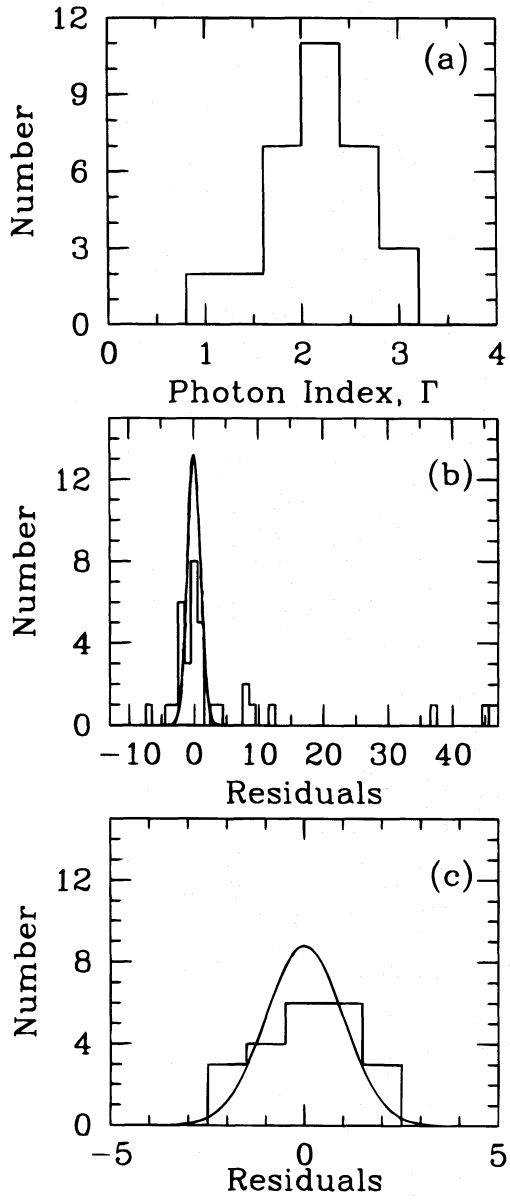

FIG. 2.—Distribution of X-ray photon indices from simple power-law fits to the PSPC spectra of the 1 Jy radio-selected sample of BL Lac objects. The column density of absorbing gas was fixed at the Galactic value except in the four cases (0426−380, 0537−441, 0716+714, and 1652+398) for which the fixed-N_H single power-law fits were unacceptable; for these the photon indices from the free-N_H fits were used. (*a*) Histogram of fitted photon indices (Table 2), with simple mean 2.16 ± 0.52 (standard deviation) and weighted mean 2.77 ± 0.01, where the latter is dominated by the brightest (and steepest) sources. (*b*) Residuals from the simple average of the distribution, expressed in individual sigmas (see text). For a homogeneous sample, this histogram should be a Gaussian centered at zero with unit dispersion (*solid line*). (*c*) Residuals when the steepest and flattest spectra ($\gtrsim 3\ \sigma$ from the average) are removed are (of course) in good agreement with the expected Gaussian.

good fit is obtained for a power law plus edge, with $E_e \sim 0.45$ keV and $\tau_e \sim 0.47$. The lower limit on the redshift ($z > 0.3$) would imply an absorption edge due to oxygen in ionization state III or higher.

The *ROSAT* spectrum of 1807+698 (3C 371) is better fitted with a concave broken power-law model, which yields a significantly reduced χ^2 ($\Delta\chi^2 = 22.9$ for 23 DOF, $P_F > 99.9\%$), with $\Delta\Gamma \approx 0.9$ above 0.7 keV, confirming a similar

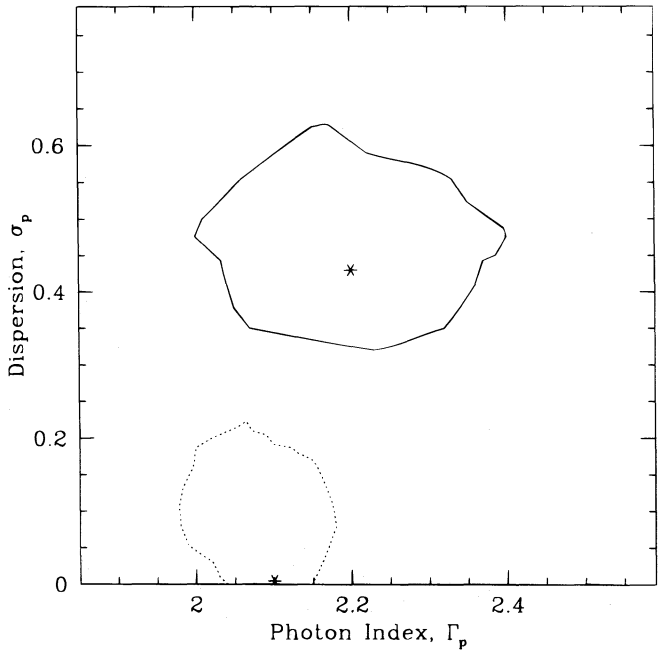

FIG. 3.—Mean PSPC spectral slope and dispersion (for fixed-N_H fits) for the 1 Jy sample of radio-selected BL Lac objects, obtained from a maximum likelihood analysis (90% confidence contour). The nonzero dispersion for the full dataset (*solid line*) indicates the sample spectra are not consistent with a single X-ray photon index. The dotted line is the contour obtained by excluding spectra more than 3 σ steeper or flatter than the mean.

result found previously for this source with *EXOSAT* (Staubert, Brunner, & Worrall 1986). A power law plus edge does not give a significantly improved fit.

3.3.3. *Cumulative Fits of Complex Models*

While simple power-law fits are a good description of the bulk of the PSPC data for the 1 Jy sample, there are reasons

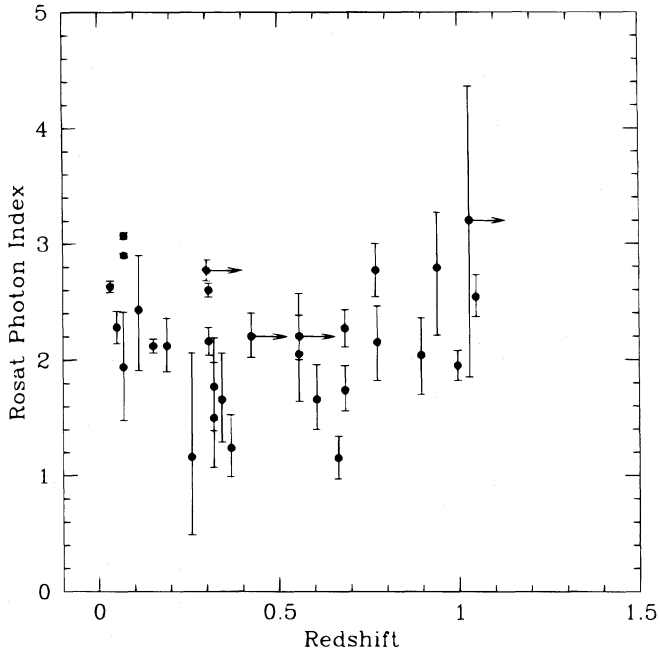

FIG. 4.—X-ray spectral slope (fixed-N_H fits) vs. redshift for the 1 Jy sample of radio-selected BL Lac objects. Arrows indicate redshift lower limits. No significant trend or correlation is present for this sample.

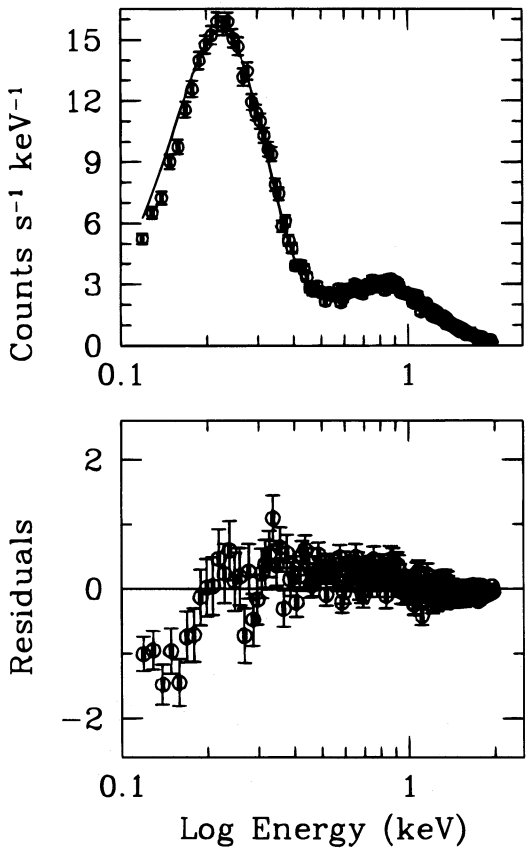

FIG. 5.—PSPC spectrum of 1652+398 (Mrk 501; *upper panel*). The residuals (data minus model) for the single power-law plus Galactic N_H fit (*lower panel*) clearly indicate a deficit of photons below 0.2 keV. A convex broken power-law model ($\Delta\Gamma = 1.3$ above 0.3 keV) gives a significantly improved fit to these data ($P_F > 99\%$).

to consider more complex models. First, the PSPC data do reveal significant deviations from a simple power law for the brightest objects, as do other, higher resolution X-ray data of BL Lac objects. Second, for the ensemble of 16 XBLs observed with *EXOSAT*, the largest such sample studied in the broad energy range 0.1–10 keV, a convex spectral model gave a significantly better fit to the ensemble of spectra than a single power law (Barr et al. 1989; Sambruna et al. 1994a, b).

Therefore, we also applied the complex models described above to the 21 spectra of the 17 sources in the 1 Jy sample for which there is no evidence of complexity in the individual spectra, and for which the redshift (or a lower limit to it) is known and the statistics are good enough (at least 10 spectral bins with ≥ 20 counts per bin). The individual χ^2-values of the various fitted models were summed in order to assess the improvement of the fits for these objects as a class.

For the broken power-law model, both spectral indices and the break energy were allowed to be free, so this model has two more free parameters (for each spectrum) than the fixed-N_H single power-law model. The total χ^2 for this model for the 21 spectra is 907.7 for 850 DOF, which is not a significant improvement with respect to the single power-law model, for which the total $\chi^2 = 940.0$ (892).

For the absorption models, we wanted to ask the particular question whether low-energy absorption by highly ionized gas (e.g., oxygen absorbing at $\sim$0.6–0.8 keV) is a ubiquitous feature for the class; we therefore limited the allowed energy range of the absorption feature in both the power law plus notch and power law plus edge models. The edge was constrained to be between the energies appropriate for O II [$E_{\rm O\,II} = 0.570/(1+z)$ keV] and O VIII [$E_{\rm O\,VIII} = 0.870/(1+z)$] keV, with the optical depth left free to vary. The resonant line was constrained to be 100 eV wide and to be centered at the redshifted energy of the oxygen Lyα absorption feature [$0.654/(1+z)$ keV]. In practice, the edge energies usually pegged at one limit or the other, so this parameter was effectively fixed and both the absorption models had one more free parameter (the optical depth) than the single power-law model.

In no individual case were the fits with the discrete absorption models (power law plus either edge or line) a significant improvement. The cumulative χ^2-values are 899.6 (871) and 914.9 (871) for the power law plus edge or line, respectively, neither of which is a significant improvement over the single power-law model.

3.4. *Spectral Variability*

Previous studies demonstrated that X-ray variability of BL Lacertae objects is common. In most cases, higher intensity states are correlated with flatter spectra (Urry et al. 1986; Sembay et al. 1993; Giommi et al. 1990; Sambruna et al. 1994a, 1995).

Six objects in our sample (0851+202, 1749+096, 1803+784, 2005−489, 2007+777, and 2254+074) were observed twice with the *ROSAT* PSPC in pointed mode. Of these, 0851+202 (OJ 287), 1803+784, and 2005−489 varied significantly between the two epochs, both in intensity and spectral shape (see Fig. 1). The intensity of 0851+202 more than doubled and its spectrum was steeper in the brighter state ($\Delta\Gamma \sim 0.4$ for fixed N_H), contrary to the established trend. The intensity of 1803+784 changed by a factor of 1.4, and the spectrum was also steeper in the higher state ($\Delta\Gamma \sim 0.6$ for fixed N_H). For 2005−489 the intensity decreased by a factor of $\sim$2 and the spectrum was flatter for the higher intensity state in the usual way ($\Delta\Gamma \sim 0.17$ for fixed N_H; Sambruna et al. 1995). For the three remaining objects (1749+096, 2007+777, and 2254+074) no variability was found (Table 1).

Inspection of Table 1 shows that 9 of the 20 1 Jy BL Lac objects detected in the *ROSAT* All-Sky Survey had count rates at least 3 σ different from the mean pointed count rates. The implied variations in intensity are as large as a factor of $\sim$6. In addition, 1514−241 varied by more than a factor of 9, and the lack of a RASS count rate for 0851+202, which is reasonably bright in our data, implies a lower intensity by a factor of $\sim$20 during the All-Sky Survey. Essentially, all the brighter objects—every 1 Jy BL Lacertae object brighter than 0.15 counts s^{-1} in the pointed data—vary significantly on long timescales, frequently with large amplitude.

Brinkmann & Siebert (1994) analyzed the RASS PSPC spectra of a group of BL Lacertae objects from the Molonglo catalog that had enough statistics for X-ray spectral analysis, including four of the objects in our sample: 1652+398, 1749+701, 1807+698, and 2005−489. Of these, 1652+398 was fainter in the survey than in the pointed observation by a factor of 1.5, and had similar spectral parameters. The RASS intensity and spectral shape of

1749+701 were similar to the values in the pointed data (within a few percent). The X-ray emission of 1807+698 dropped by a factor of 1.8 between the RASS (Fink et al. 1992) and the pointed observation, without a significant change in the spectrum. The RASS spectrum of 2005−489 corresponded to a brightness similar to the higher state of the pointed observations, with similar fitted N_H but steeper slope ($\Gamma = 3.46 \pm 0.28$) than for the pointed spectrum.

In summary, pointed data for two sources (0851+202 and 1803+784) yield steeper spectra in the brighter state, while one (2005−489) is flatter in the brighter state. It is interesting to note that the latter object is an "XBL-like" RBL—Padovani & Giommi (1996) define these as "high-frequency break BL Lacertae objects," or HBLs, because the X-ray flux to radio flux density ratio is $f_x/f_r < 10^{-11.5}$ ergs cm^{-2} Jy^{-1}, where f_x is the flux in the 0.3–3.5 keV energy band and f_r is the flux density at 5 GHz, or equivalently, $\alpha_{rx} < 0.8$ (most XBLs in existing samples are HBLs). Like other HBLs, 2005−489 follows the usual trend of flatter spectrum in the brighter mode. Our results suggest the opposite trend (steeper in the brighter state) holds for the RBL-like objects ($\alpha_{rx} > 0.8$, which Padovani & Giommi 1996 call "low-frequency break BL Lacertae objects," or LBLs).

4. COMPARISONS WITH OTHER X-RAY SPECTRAL STUDIES

In this section, we compare our PSPC results to PSPC pointed observations of the complete XBL sample of the Extended Medium Sensitivity Survey (Perlman et al. 1996a) and a small but complete sample of eight strong emission-line blazars (FSRQs; Brunner et al. 1994) drawn from the S5 radio sample, which includes all radio sources with declination $\geq 70°$ and Galactic latitude greater than 10° brighter than 1 Jy at 5 GHz (Kühr et al. 1981). We also compare the PSPC spectra with IPC spectra for a subset of the 1 Jy sample of RBLs. Finally, we compare the soft X-ray results with the limited observations of RBLs at higher energies.

4.1. *Comparison of Radio-Selected BL Lac Objects with Other Blazars*

The distribution of soft X-ray spectral indices for the EMSS XBLs (Fig. 6*a*, *dotted line*) and the 1 Jy RBLs (*solid line*) span a similar range, $\Gamma \sim 1$–3, and are not demonstrably different according to a K-S test (probability the two distributions are the same, $P_{K\text{-}S} \sim 85\%$). The means and standard deviations for the two samples, $\langle \Gamma_{RBL} \rangle = 2.17 \pm 0.52$ for the 33 1 Jy RBLs and $\langle \Gamma_{XBL} \rangle = 2.30 \pm 0.49$ for the 23 EMSS XBLs, are consistent according to a Student's *t*-test.

However, if we divide the samples according to their radio to X-ray flux ratios, (using the revised dividing point $\alpha_{rx} = 0.8$ suggested by Padovani & Giommi 1996 and α_{rx} indices from Sambruna et al. 1996), the LBLs (which are the 1 Jy RBLs minus five objects) have significantly flatter soft X-ray spectra than the HBLs (the XBLs plus the five RBLs), as shown in Figure 6*b*. The K-S probability that the two distributions are similar is only $P_{K\text{-}S} \sim 3.0\%$ and the mean indices, $\langle \Gamma_{LBL} \rangle = 2.04 \pm 0.49$ and $\langle \Gamma_{HBL} \rangle = 2.40 \pm 0.48$, differ at 99.2% confidence according to the Student *t*-test. Similar results were found by Comastri et al. (1996) and Padovani & Giommi (1996).

Table 3 summarizes the average photon indices for each sample. In Figure 6*b* we also show the distribution of PSPC spectral indices (*dashed line*) for the FSRQ sample of Brunner et al. (1994). The soft X-ray spectra of FSRQs are flatter than for LBLs and HBLs, with K-S probabilities of

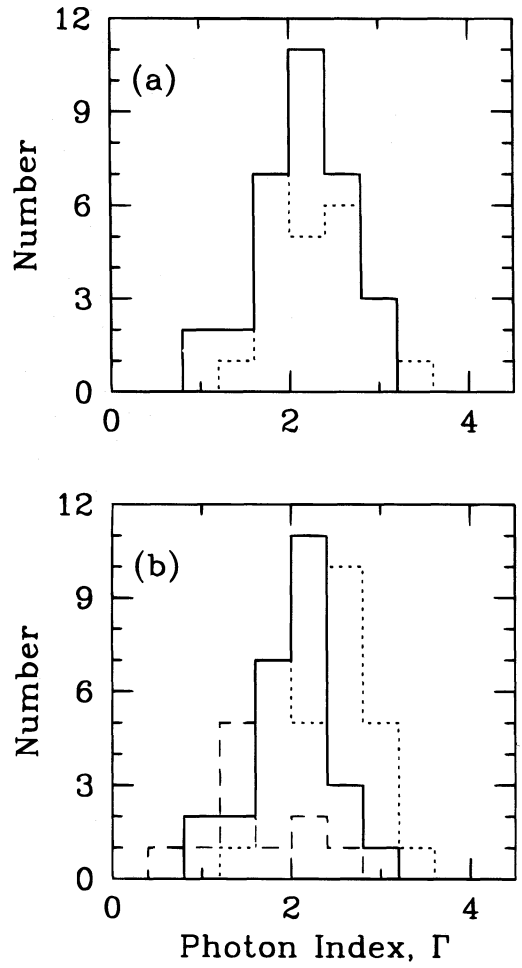

FIG. 6.—X-ray spectral index distributions for three complete samples of blazars observed with the *ROSAT* PSPC. (*a*) *solid line*, 1 Jy sample of radio-selected BL Lac objects (present work); *dotted line*, EMSS X-ray–selected BL Lac objects (Perlman et al. 1996a). (*b*) *solid line*, LBLs (or "low-frequency peaked BL Lacertae objects") from the 1 Jy sample of RBLs; *dotted line*, HBLs (or "high-frequency peaked BL Lacertae objects") from the EMSS (which contains no LBLs); *dashed line*, complete sample of eight flat-spectrum radio quasars drawn from the S5 radio sample (Brunner et al. 1994). The FSRQs are flatter than the LBLs, which are flatter than the HBLs.

TABLE 3

AVERAGE *ROSAT* PHOTON INDICES

OBJECT	SIMPLE	WEIGHTED	MAXIMUM LIKELIHOOD[a]	
			Γ_p	σ_p
RBL	2.17 ± 0.52	2.75 ± 0.01	$2.20^{+0.18}_{-0.22}$	$0.43^{+0.20}_{-0.20}$
XBL[b]	2.30 ± 0.49	2.37 ± 0.04	$2.30^{+0.25}_{-0.22}$	$0.40^{+0.23}_{-0.13}$
LBL.....	2.04 ± 0.49	2.22 ± 0.03	$2.08^{+0.17}_{-0.23}$	$0.35^{+0.17}_{-0.15}$
HBL	2.40 ± 0.48	2.82 ± 0.01	$2.40^{+0.22}_{-0.18}$	$0.44^{+0.16}_{-0.10}$
FSRQ[c].....	1.54 ± 0.56	1.48 ± 0.03	$1.60^{+0.25}_{-0.35}$	$0.34^{+0.36}_{-0.21}$

[a] Errors at 90% confidence.
[b] Data from Perlman et al. 1995.
[c] Data from Brunner et al. 1994.

6.24% and 0.33%, respectively, that the spectral index distributions are drawn from the same parent distribution. The mean photon index for FSRQs, $\langle \Gamma_{\rm FSRQ} \rangle = 1.54 \pm 0.56$, differs from the LBLs and HBLs mean indices at 98.86% and 99.99% confidence, respectively, according to a Student's t-test. (The difference between FSRQs and RBLs or XBLs is greater, ~99.9% confidence, like the result found by Brunner et al. [1994] for eight FSRQs and five RBLs from the S5 radio sample.)

We compared the intrinsic distributions of the photon indices for the three blazar classes using the maximum likelihood method (Worrall 1989), as shown in Figure 7. Panel (*a*) shows the 90% confidence contours for photon index and dispersion for the 1 Jy RBLs sample (*solid line and asterisk*) and the EMSS XBLs sample (*dotted line and square*); the means are not significantly different. The difference is significant, however, for LBLs and HBLs (Fig. 7*b*, *solid and dotted lines*), with LBLs being significantly flatter. The FSRQs (Fig. 7*b*, *dashed line*) are still flatter than the LBLs. Figure 7*b* shows clearly that LBLs have soft X-ray spectra intermediate between HBLs and FSRQs.

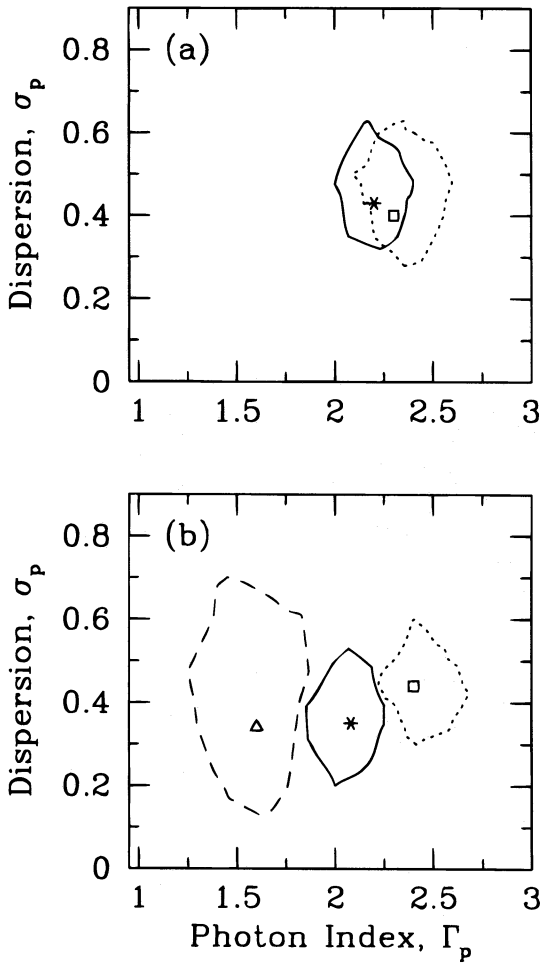

FIG. 7.—Mean PSPC photon indices and dispersions for blazars obtained from a maximum likelihood analysis. (*a*) Comparison of the 1 Jy sample of radio-selected BL Lac objects (*solid line and star*) and the EMSS sample of X-ray–selected BL Lac objects (*dotted line and square*). The soft X-ray spectral parameters for the two BL Lac samples are not significantly different. (*b*) Comparison of "low-frequency peaked BL Lacertae objects" (LBLs; *solid line and asterisk*), "high-frequency peaked BL Lacertae objects" (HBLs; *dotted line and square*), and flat-spectrum radio-loud quasars from the S5 radio sample (FSRQs; *dashed line and triangle*). The X-ray spectra of the three classes are significantly different at 90% confidence, with LBLs steeper than FSRQs and flatter than HBLs.

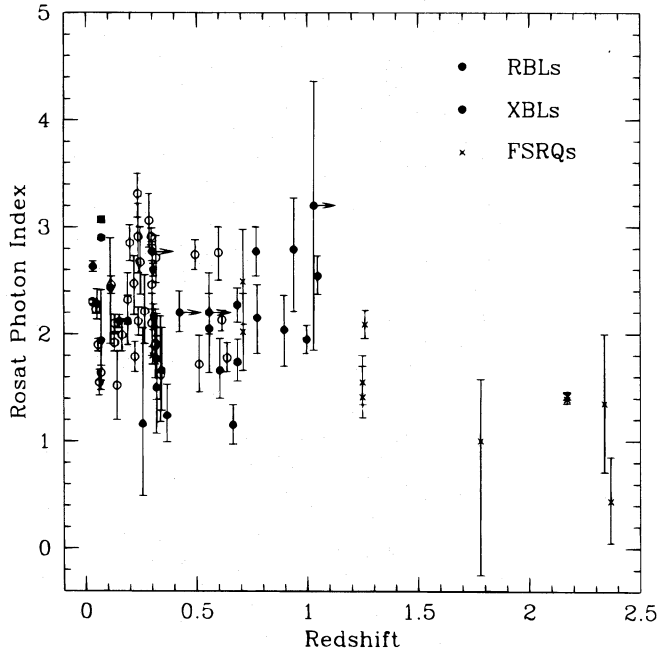

FIG. 8.—X-ray spectral slope vs. redshift for three complete samples of blazars: *filled circles*, 1 Jy sample of radio-selected BL Lac objects (present work); *open circles*, EMSS X-ray–selected BL Lac objects (Perlman et al. 1996a); *crosses*, complete sample of eight flat-spectrum radio quasars from the S5 survey (Brunner et al. 1994). Over this large redshift range, there is a significant trend for more distant quasars to have significantly flatter X-ray spectra than more local BL Lac objects ($P > 99.9\%$, Kendall nonparametric test).

The different X-ray slopes of BL Lac objects and emission-line blazars may be related to their different redshift distributions. Figure 8 shows the PSPC photon indices for complete samples of RBLs (*filled circles*), XBLs (*open circles*), and FSRQs (*crosses*) versus their redshifts. In contrast to the situation for RBLs alone (Fig. 4), the correlation with redshift is significant at more than 99.9% confidence (Kendall's tau nonparametric test), in the sense that more distant sources have flatter spectra. This correlation, which is clearly introduced by the FSRQ sample (99% correlation probability for this sample alone), suggests the onset of a flat Compton-scattered component at ~1 keV that for objects at large redshift ($z > 1$) increasingly dominates the observed soft X-ray band. Alternatively, the presence of strong emission lines in FSRQs may indicate physical differences associated with the production of a hard X-ray continuum, such as the presence of an accretion disk with a hot corona.

4.2. *IPC Measurements of the X-ray Spectra of Radio-Selected BL Lac Objects*

Thirteen of the 1 Jy RBLs were observed previously with the *Einstein Observatory* Imaging Proportional Counter (IPC), which was sensitive in a slightly harder range, 0.3–3.5 keV, and had somewhat lower sensitivity and spectral resolution than the *ROSAT* PSPC. These data have been analyzed by Worrall & Wilkes (1990), together with the IPC

spectra of other blazars, but only free-N_H fits were published. The IPC spectral indices have very large uncertainties, mostly due to the lower sensitivity of the IPC experiment with respect to the *ROSAT* PSPC. To minimize the uncertainties and to permit a uniform comparison with our study, we reanalyzed the archival IPC data for the 13 objects common to the IPC and PSPC samples of RBLs, fitting the data with a single power law and fixed (Galactic) N_H. As in the case of the *ROSAT* data, repeated observations of a single object were considered individually.

As shown in Figure 9, the IPC spectral indices are systematically flatter than the PSPC indices. The simple mean photon index for the IPC is $\langle\Gamma_{IPC}\rangle = 1.74 \pm 0.38$, compared to $\langle\Gamma_{PSPC}\rangle = 2.10 \pm 0.40$ for the PSPC. The two values differ at the 99% confidence level (Student's t-test) and the K-S probability that the two distributions are consistent is only $\sim$2.8%. A maximum likelihood analysis (Fig. 10) confirms that the IPC spectra are significantly flatter than the PSPC spectra. The dispersion in the IPC case is consistent with zero, i.e., the IPC distribution is consistent with a single value of the spectral slope; this is largely because the uncertainties in the IPC spectral indices are larger than for the PSPC indices.

We considered possible systematic causes of the spectral differences. The flatness of the IPC slopes is unlikely to be due to source variability. If the flux densities obtained with the PSPC and the IPC are compared (Fig. 11), long-term variability is apparent for several sources, but there is no systematic difference in intensity with observing instrument.

The IPC slopes of a mixed sample of 18 radio-loud and radio-quiet quasars are also significantly flatter than those measured with *ROSAT* (Fiore et al. 1994, and references therein), and it has been suggested that this systematic difference is due to a different calibration of the spectral responses of the two satellites (Fiore et al. 1994). Alternatively, soft excesses may be present in these active galactic nuclei (Turner & Pounds 1989; Masnou et al. 1992; Urry et al. 1989; Shastri et al. 1993).

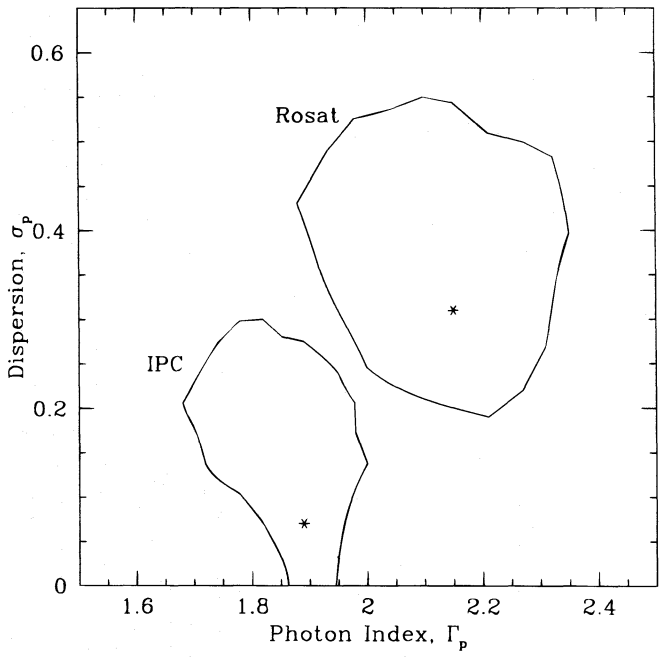

FIG. 10.—Mean X-ray spectral indices and dispersions for the subsample of 13 1 Jy radio-selected sample of BL Lac objects that were observed with both the *ROSAT* PSPC and the *Einstein Observatory* IPC, from a maximum likelihood analysis (90% confidence). The IPC indices are significantly flatter than the PSPC indices; that the former are consistent with zero dispersion is largely due to the greater uncertainties in the IPC measurements.

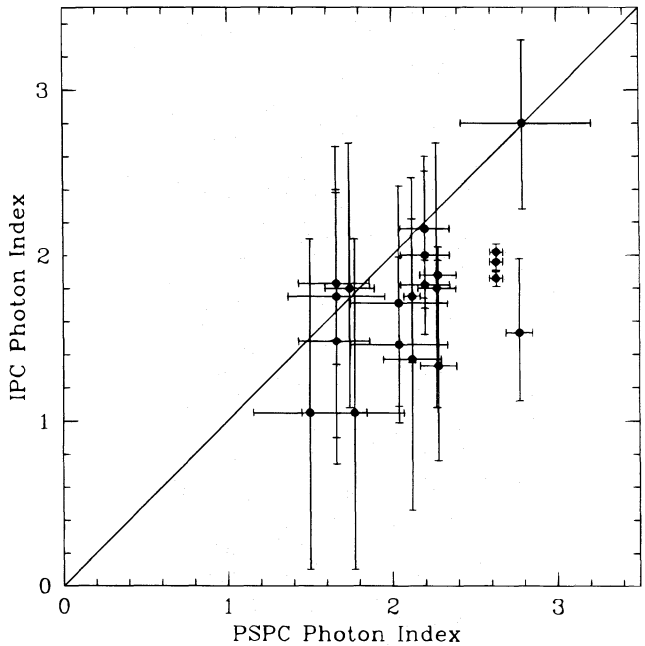

FIG. 9.—Comparison of X-ray spectral indices of 1 Jy BL Lac objects determined with the *ROSAT* PSPC and the *Einstein Observatory* IPC, for fixed-N_H single power-law fits. The PSPC indices are systematically steeper than the IPC indices, indicating spectral flattening at $\sim$1 keV for the sample as a whole.

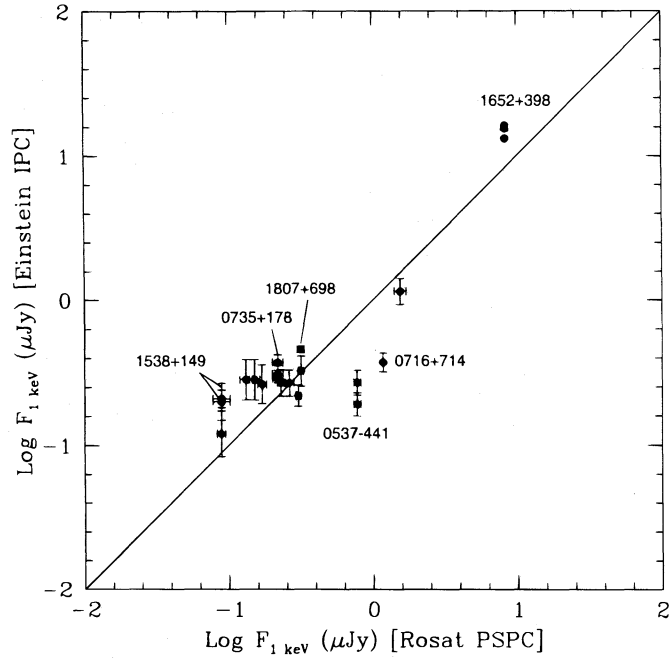

FIG. 11.—Long-term X-ray variability of the 1 Jy sample of radio-selected BL Lac objects. The IPC flux densities at 1 keV are compared to the flux densities measured with the *ROSAT* PSPC (error bars are 90% confidence). Four sources varied significantly between the two epochs, but there is no trend for the IPC and PSPC to measure systematically different fluxes.

We extracted and compared PSPC and IPC spectra for HBLs and FSRQs for which both PSPC and IPC archival data were available. The HBLs, only four objects, were taken from the *HEAO 1* Large Area Sky Survey (Remillard et al. 1996) as the EMSS objects are too faint to have well constrained spectra. The four FSRQs are from the sample from Brunner et al. (1994) and from the Pearson & Readhead (1988) list. For these two other blazar types, we find no systematic difference in spectral slopes between the PSPC and the IPC. Comparisons involving more objects are clearly desirable, but based on available data we conclude that the difference in spectral shapes for the 1 Jy RBLs is intrinsic and results from the different energy ranges covered by the PSPC and IPC instruments.

The flatness of the IPC spectra of RBLs compared to the PSPC spectra suggests that a flat, Compton-scattered component in RBLs dominates the steep synchrotron component in the IPC but is comparable to the synchrotron component in the PSPC. For a spectral index $\Gamma \sim 2.2$, the mean effective energy of the PSPC is ~ 0.3 keV, while for the IPC it is ~ 0.9 keV. Thus, the difference in IPC and PSPC spectra of RBLs suggests that the equal intensity point for synchrotron and Compton components is near ~ 1 keV.

4.3. *Hard X-Ray Spectra of Radio-Selected BL Lac Objects*

Data at higher energies ($\gtrsim 2$ keV) are scarce for radio-selected BL Lac objects because of their relative faintness in X-rays. Several significant detections with *HEAO 1* have been reported (Schwartz et al. 1989), although for only one RBL, 1652+398 (Mrk 501), is there published spectral information (and this object is in fact an HBL, with peak synchrotron emission at UV/X-ray wavelengths). The hard ($\gtrsim 2$ keV) spectrum of 1652+398 has a rather variable slope, with reported photon indices in the range 1.2–2.6 (Urry et al. 1986), and *EXOSAT* observations showed a spectral flattening of $\Delta\Gamma \sim 0.4$ for a factor of 4 increase in flux (Giommi et al. 1990; Sambruna et al. 1994a, b).

Five 1 Jy RBLs (0537−441, 0851+202, 1652+398, 1807+698, and 2005−489) were detected with *EXOSAT* at $\gtrsim 2$ keV (Giommi et al. 1990), and the range spanned by their photon indices is quite large, from $\Gamma = 1.3$ for 0537−441, to $\Gamma = 3.7$ for 2005−489 in the low state, to an exceptionally steep slope ($\Gamma \sim 5$) for 0851+202 (OJ 287) on one occasion (Sambruna et al. 1994a, b). Note that 1652+398 and 2005−489 are both HBLs. Only one 1 Jy RBL was detected by *Ginga*, 2200+420 (BL Lac; Kawai et al. 1991), with a rather flat and variable spectrum ($\Gamma \sim 1.7$–2.2). Repeated hard X-ray observations of individual RBLs reveal the usual trend of flatter spectra in higher intensity states, in contrast to their behavior in the PSPC data (see § 3.4).

5. SUMMARY AND DISCUSSION

Our survey of the complete 1 Jy sample of radio-selected BL Lac objects with the *ROSAT* PSPC shows that their soft X-ray spectra are in general well fitted by a simple power-law model modified for absorption in the interstellar medium of our Galaxy. The spectra are quite soft, with an average photon index $\langle\Gamma\rangle = 2.16 \pm 0.52$, but the ensemble cannot be described by a single spectral slope and must have an intrinsic dispersion.

The distribution of PSPC indices for the 1 Jy sample of radio-selected BL Lac objects is similar to that of the X-ray–selected BL Lac objects from the Extended Medium Sensitivity Survey (Perlman et al. 1996a), but dividing the samples slightly differently, into LBLs ("low-frequency peaked BL Lacertae objects") and HBLs ("high-frequency peaked BL Lacertae objects") based on their broad-band spectral properties, we find that the LBLs have significantly flatter soft X-ray spectra than the HBLs. Furthermore, both LBLs and HBLs (and RBLs and XBLs) spectra are steeper than those of higher-redshift flat-spectrum radio quasars (Brunner et al. 1994).

The X-ray spectral properties of the RBL sample, particularly the large dispersion in power-law slopes, suggests that radio selection picks objects intermediate between XBLs and FSRQs. The RBLs are a potential link with the so-called "intermediate blazars" (Kollgaard 1994) and may indicate a physical connection important to the whole blazar class (Sambruna et al. 1996).

Five of the brightest sources in our RBL sample were better fitted by more complex spectral models than a single power law. In two cases this was probably because of unrelated intervening absorption. For 0235+164, the addition of a cold absorber ($N_H \sim 4.3 \times 10^{21}$ cm^{-2}) at $z = 0.524$, the redshift of a known intervening absorption system, provides a significantly better fit to the PSPC data. For 0426−380, a cold absorber at $z = 1.03$ improves the fit, but the PSPC spectrum is too faint to allow us to distinguish between that model and a broken power law.

In the other three cases, the spectra appear to show excess absorption and/or changes in continuum shape. The PSPC spectrum of 1652+398 (Mrk 501), for which more than 40,000 counts were detected, is significantly better fit by a broken power-law model steeper by $\Delta\Gamma \sim 1.3$ above 0.3 keV. In contrast, 0716+714 has a concave spectrum, caused either by spectral flattening of $\Delta\Gamma \sim 0.5$ above 0.5 keV or an absorption edge at $E_e = 0.45$ keV with optical depth $\tau \sim 0.5$. Similarly, in 1807+698 the PSPC spectrum flattens by $\Delta\Gamma \sim 0.9$ above 0.7 keV.

For the remaining 1 Jy RBLs, the quality of the PSPC data is insufficient to justify more complex spectral models. We did search via a cumulative analysis (excluding the brightest sources) for evidence of similar spectral curvature or common absorption features but did not find any significant deviations from a simple power law.

Some of the 1 Jy RBLs with the steepest and flattest X-ray spectra have properties that set them apart from the other RBLs. For example, the steep X-ray sources 1652+398 and 2005−489 are similar to X-ray–selected BL Lacertae objects in their low radio to X-ray ratio and their characteristic X-ray hardening with increasing intensity in the 0.1–10 keV range (Sambruna et al. 1995, 1994a, b). In contrast, the flattest 1 Jy sources have properties more consistent with those of quasars. Broad emission lines have been detected in the optical spectra of 1803+784 and 1823+568 (with equivalent widths 51 and 19 Å), while somewhat weaker optical lines have been seen from 0954+658 (Stickel, Fried, & Kühr 1993). Two RBLs, 0954+658 and 1823+568, have edge-brightened radio morphologies, more like quasars than other BL Lac objects (Kollgaard et al. 1992), and also have unusually high superluminal speeds (Gabuzda & Sitko 1994). Finally, 0954+658 is one of the most polarized blazars in the radio, with parsec-scale polarization nearly perpendicular to the jet

axis, while other RBLs typically have parallel polarization (Gabuzda et al. 1992). Removing those BL Lac objects with detected broad lines and/or edge-brightened radio morphologies reduces the dispersion in X-ray spectral slope.

While the spectral slopes of the RBL sample are similar to those of the XBLs, their spectral variability may be different. Three of the six BL Lac objects pointed at more than once with the PSPC varied both in intensity and spectral shape. In one case, 2005−489, the *ROSAT* PSPC spectrum is flatter in the higher intensity state, as is typical of XBLs (see also Sambruna et al. 1995). This object has a broadband continuum shape much more like XBLs than the other RBLs, with a peak synchrotron frequency near UV frequencies. In marked contrast, 0851+202 and 1803+784, show the unusual trend of steeper spectra with higher intensity. This can be explained if their low state spectra were dominated by flat Compton components, while the high state spectra were dominated by the steeper synchrotron component. In this case, the flattening of the synchrotron component with increasing intensity is a smaller effect than the swamping of the very flat Compton component.

The 13 RBLs observed with both the *ROSAT* PSPC and the *Einstein Observatory* IPC have flatter spectra in the IPC data (0.3–3.5 keV) than in the PSPC data (0.1–2.0 keV). This also suggests the onset of a flatter component around ~1 keV, significant in the RBLs but apparently not in the XBLs. That is, spectral hardening with energy, together with the large intrinsic dispersion in soft X-ray spectral indices for RBLs and the relative X-ray spectral slopes of the different kinds of blazars, suggests that synchrotron emission dominates the X-ray spectrum of both radio-selected and X-ray–selected BL Lac objects, while a Compton-scattered component (probably extending all the way to gamma-ray energies in some cases) dominates in emission-line blazars. For many of the RBLs if not for the XBLs, the intensity of the two components in the PSPC band must be comparable, as evidenced in particular by the large intrinsic dispersion in spectral indices. The approximate energy for the onset of the Compton-scattered component in RBLs must be $\gtrsim 1$ keV, and substantially less (<0.5 keV) in emission-line blazars. The convex spectra of XBLs as measured with *EXOSAT* above 2 keV, suggest that in this class of blazars the Compton component should arise at still larger energies ($\gtrsim 10$ keV). In 2005−489, for example, which has a 4 σ γ-ray detection (von Montigny et al. 1995), a Compton component arises at $\gtrsim 40$ keV (Sambruna et al. 1995).

Rapid X-ray variability was detected in three of the BL Lac objects studied. Doubling timescales were a week or less (in one case as short as ~8 hr), and detected amplitudes were as large as a factor of 7. The relatively short duration of the PSPC observations, typically a few thousand seconds, and the satellite wobble with its period of ~400 s severely limit (on long and short timescales, respectively) the range of variability timescales to which the pointed data were sensitive. The PSPC data do not contradict the notion that rapid X-ray variability in radio-selected BL Lac objects is quite common.

In addition, half the 1 Jy BL Lac objects detected in the *ROSAT* All Sky Survey were clearly variable between the scanning and pointed observations; the half that were not clearly variable were also fainter. Thus, our observations are consistent with the idea that all radio-selected BL Lacertae objects vary on timescales of months to years.

R. M. S. acknowledges support from NASA grants NAG 5-1918 and NAG 5-2510, D. M. W. acknowledges support from NASA grant NAG 5-1724, and R. I. K. and E. D. F. acknowledge support from NASA grant NAGW-2120. We are grateful to Renato Falomo and Joe Pesce for their help with the Supermongo macro for Figure 1.

APPENDIX A

ESTIMATION OF H I COLUMN DENSITY TOWARD SOUTHERN SOURCES

At least some part of the absorption in X-ray spectra of extragalactic objects must come from Galactic interstellar gas along the line of sight. To evaluate the appropriate contribution from our Galaxy, we use 21 cm measurements of H I in emission. These are generally available in the northern hemisphere, especially with the large Bell Labs survey of Stark et al. (1992), but not at declinations $\delta < -39°$.

To estimate N_H for sources not covered by the Bell Labs survey, we devised the following scheme (following work by P. Giommi 1995, private communication). We used the Bell Labs survey data to determine N_H on a grid of Galactic latitude and longitude, with at least 50 points per latitude (binned at 5°), then fitted a smooth function in latitude.

Figure 12 shows the log of the H I column density (taken from Stark et al. 1992) versus Galactic latitude, for a range of Galactic longitudes (shown with different symbols for each quadrant). No trends are apparent as a function of longitude (not shown), and so the scatter of the points yields the uncertainty of N_H for a fixed latitude. Figure 13 shows the mean N_H, averaged over longitude for fixed latitudes and with the corresponding standard deviation, plotted versus latitude. Because of the approximate symmetry around $b = 0°$, we fitted the region $b \geq 0°$, where there are few gaps in the sky coverage, and reflected the results about $b = 0°$ to cover the negative latitudes.

No single polynomial can easily fit the whole region $b \geq 0°$. While the points for $b < 20°$ require a polynomial of order ≥ 4, the points for $b \geq 20°$ are adequately represented by the linear function (shown in Fig. 13):

$$N_H(10^{20}\mathrm{cm}^{-2}) = (5.806 \pm 1.050) - (0.0546 \pm 0.0145)|b| . \quad \text{(A1)}$$

We use this equation to get N_H for two BL Lacertae objects with no other appropriate data, 2005−489 and 0537−441. For both 2005−489, at $b = -32°$, and 0537−441, at $b = -31.°09$, we obtain $N_H = 4.1 \times 10^{20}$ cm^{-2}. The uncertainties in N_H are large—roughly 3×10^{20} cm^{-2} (from Fig. 13) in contrast to the 1×10^{20} cm^{-2} estimated for the Bell Labs survey or 1×10^{19}

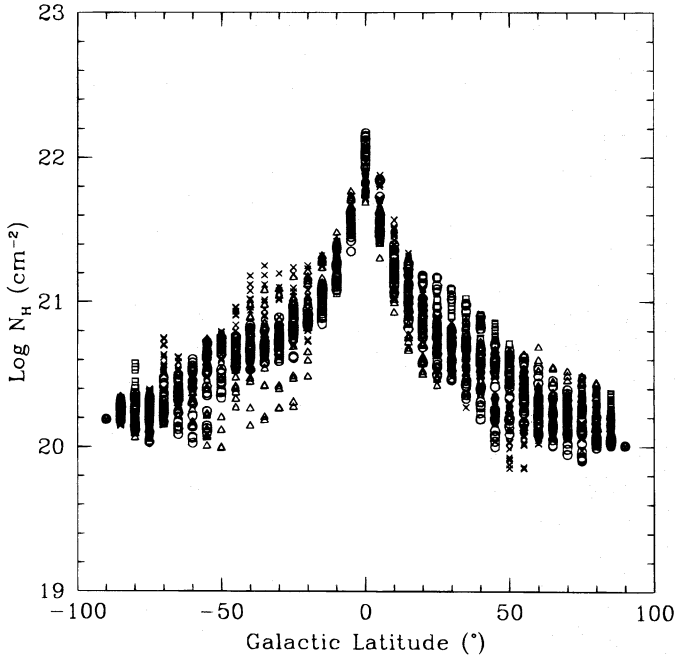

FIG. 12.—H I column density (Stark et al. 1992) vs. Galactic latitude, for a range of longitudes (l). *Open circles:* $0° \leq l \leq 90°$; *crosses:* $95° \leq l \leq 180°$; *open triangles:* $185° \leq l \leq 270°$; *open squares:* $275° \leq l \leq 360°$. There is no smooth trend in longitude; the scatter of the points at a given latitude represents real fluctuations in N_H over the sky, so we take the rms about the mean to represent the uncertainty in estimated values of N_H.

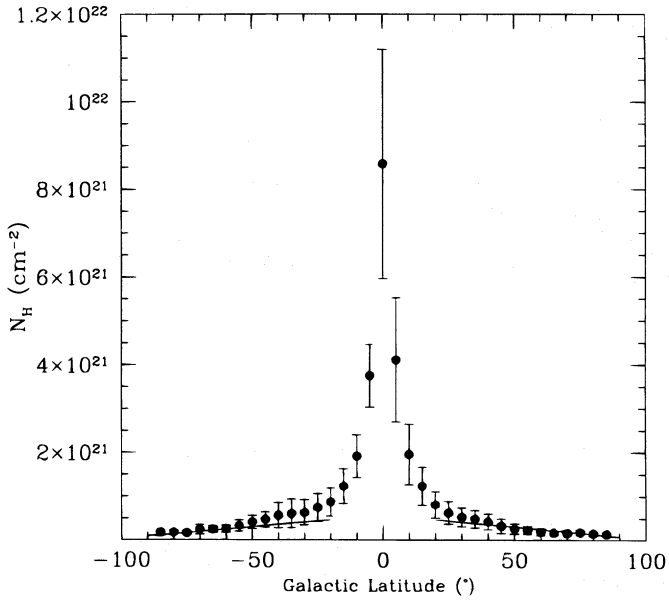

FIG. 13.—Mean H I column density averaged over longitude vs. latitude, with 1 σ uncertainties from the standard deviation about the mean. The linear fit given by eq. (A1) is shown as a solid line.

cm^{-2} for the Elvis et al. (1989) measures—but in the absence of easily accessible H I maps (integrated over all velocities, which may not happen in surveys for high-velocity clouds), equation (A1) gives a useful approximation for $|b| \geq 20°$.

REFERENCES

Barr, P., Giommi, P., Pollock, A., Tagliaferri, G., Maccagni, D., & Garilli, B. 1989, in BL Lac Objects, ed. L. Maraschi, T. Maccacaro, & M.-H. Ulrich (Berlin: Springer), 267
Bechtold, J., et al. 1994, AJ, 108, 759
Briel, U. G., et al. 1994, The *ROSAT* Users' Handbook, working draft
Brinkmann, W., & Siebert, J. 1994, A&A, 285, 812
Brunner, H., Dörrer, T., Friedrich, P., Lamer, G., & Staubert, R. 1993, AIT preprint 7/93
Brunner, H., Lamer, G., Worrall, D. M., & Staubert, R. 1994, A&A, 287, 436
Canizares, C. R., & Kruper, J. 1984, ApJ, 278, L99
Cappi, M., Comastri, A., Molendi, S., Palumbo, G. G. C., Della Ceca, R., & Maccacaro, T. 1994, MNRAS, 271, 438
Comastri, A., Molendi, S., & Ghisellini, G. 1996, MNRAS, 277, 297
Elvis, M., et al. 1992, ApJS, 80, 257
Elvis, M., Lockman, F. J., & Wilkes, B. J. 1989, AJ, 97, 777
Fink, H. H., et al. 1992, MPE Report 235, 181
Fink, H. H., Thomas, H.-C., Hasinger, G., Predhel, P., Schaeidt, S., Makino, F., & Warwick, R. S. 1991, A&A, 246, L6
Fiore, F., Elvis, McDowell, J. C., Siemiginowska, A., & Wilkes, B. J. 1994, ApJ, 431, 515
Fried, J. W., Stickel, M., & Kühr, H. 1993, A&A 268, 53
Fruscione, A. 1996, ApJ, 459, 509
Gabuzda, D. C., Cawthorne, T. V., Roberts, D. H., & Wardle, J. F. C. 1992, ApJ, 388, 40
Gabuzda, D. C., & Sitko, M. L. 1994, AJ, 107, 884

Ghisellini, G., Maraschi, L., Tanzi, E. G., & Treves, A. 1986, ApJ, 310, 317
Giommi, P., Barr, P., Garilli, B., Maccagni, D., & Pollack, A. M. T. 1990, ApJ, 356, 432
Giommi, P., & Padovani, P. 1994, MNRAS, 268, L51
Jannuzi, B. T., Smith, P. S., & Eaton, R. 1994, ApJ, 428, 130
Kawai, N., et al. 1991, ApJ, 382, 508
Kollgaard, R. I. 1994, Vistas Astron., 38, 29
Kollgaard, R. I. Wardle, J. F. C., Roberts, D. H., & Gabuzda, D. C. 1992, AJ, 104, 1687
Kühr, H., Witzel, A., Pauliny-Toth, I. I. K., & Nauber, U. 1981, A&AS, 45, 367
Ledden, J. E., & O'Dell, S. L. 1985, ApJ, 298, 630
Madejski, G. M. 1994, ApJ, 432, 554
Madejski, G. M., et al. 1996a, ApJ, 459, 156
———. 1996b, ApJ, submitted
Madejski, G. M., Mushotzky, R. F., Weaver, K. A., Arnaud, K. A., & Urry, C. M. 1991, ApJ, 370, 198
Madejski, G. M., & Schwartz, D. A. 1989, in BL Lac Objects, ed. L. Maraschi, T. Maccacaro, & M.-H. Ulrich (Berlin: Springer), 267
Maraschi, L., Fossati, G., Tagliaferri, G., & Treves, A. 1995, ApJ, 443, 578
Maraschi, L., Ghisellini, G., Tanzi, E. D., & Treves, A. 1986, ApJ, 310, 325
Marshall, H. L., Fruscione, A., & Carone, T. E. 1995, ApJ, 439, 90
Masnou, J. L., Wilkes, B. J., Elvis, M., McDowell, J. C., & Arnaud, K. A. 1992, A&A 253, 35
Morris, S. L., Stocke, J. T., Gioia, I. M., Schild, R. E., Wolter, A., Maccacaro, T., & Della Ceca, R. 1991, ApJ, 380, 49
Morrison, R., & McCammon, D. 1983, ApJ, 270, 119
Ohashi, T. 1989, in BL Lac Objects, ed. L. Maraschi, T. Maccacaro, & M.-H. Ulrich (Berlin: Springer), 296
Padovani, P., & Giommi, P. 1995, ApJ, 444, 567
———. 1996, MNRAS, in press
Pearson, T. J., & Readhead, A. C. S. 1988, ApJ, 328, 114
Perlman, E., Stocke, J. T., Wang, Q. D., & Morris, S. 1996a, ApJ, 456, 451
Perlman, E. S., et al. 1996b, ApJ, in press
Pesce, J. E., Falomo, R., & Treves, A. 1994, AJ, 107, 494
Quirrenbach, A., et al. 1989, Nature, 337, 442
Remillard, R. A., et al. 1996, ApJ, in press
Sambruna, R. M., Barr, P., Giommi, P., Maraschi, L., Tagliaferri, G., & Treves, A. 1994a, ApJ, 434, 468
———. 1994b, ApJS, 95, 371
Sambruna, R. M., Maraschi, L., & Urry, C. M. 1996, ApJ, 463, 444
Sambruna, R. M., Urry, C. M., Ghisellini, G., & Maraschi, 1995, ApJ, 449, 567
Schachter, J. F., et al. 1993, ApJ, 412, 541
Schwartz, D. A., Brissenden, R. J. V., Tuohy, I. R., Feigelson, E. D., Hertz, P. L., & Remillard, R. A. 1989, in BL Lac Objects, ed. L. Maraschi, T. Maccacaro, & M.-H. Ulrich (Berlin: Springer), 209
Sembay, S., et al. 1993, ApJ, 404, 112
Shastri, P., Wilkes, B. J., Elvis, M., & McDowell, J. 1993, ApJ, 410, 29
Smith, E. P., O'Dea, C. P., & Baum, S. A. 1995, ApJ, 441, 113
Stark, A. A., Gammie, C. F., Wilson, R. W., Bally, J., Linke, R. A., Heiles, C., & Hurwitz, M. 1992, ApJS, 79, 77
Staubert, R., Brunner, H., & Worrall, D. M. 1986, ApJ, 310, 694
Stein, W. A., O'Dell, S. L., & Strittmatter, P. A. 1976, ARA&A, 14, 173
Stickel, M., Fried, J. W., & Kühr, H. 1993, A&AS, 98, 393
Stickel, M., Padovani, P., Urry, C. M., Fried, J. W., & Kühr, H. 1991, ApJ, 374, 431
Stocke, J. T., Liebert, J., Schmidt, G., Gioia, I., Maccacaro, T., Schild, R., Maccagni, D., & Arp, H. 1985, ApJ, 298, 619
Stocke, J. T., Morris, S. L., Gioia, I. M., Maccacaro, T., Schild, R., Wolter, A., Fleming, T. A., & Henry, J. P. 1991, ApJS, 76, 813
Tashiro, M., Ueda, Y., Kii, T., Makino, F., Mushotzky, R. F., Makishima, K., & Yamashita, A. 1994, in New Horizons of X-Ray Astronomy, ed. F. Makino & T. Ohashi (Tokyo: Universal Academy Press), 343
Treves, A., Belloni, T., Falomo, R., Fink, H., Maraschi, L., Sambruna, R. M., Tagliaferri, G., & Zimmermann, H. O. 1993, ApJ, 406, 447
Turner, T. J., & Pounds, K. A. 1989, MNRAS, 240, 833
Urry, C. M., Arnaud, K. A., Edelson, R. A., Kruper, J. S., & Mushotzky, R. F. 1989, in AGN and the X-Ray Background, ed. N. E. White (ESA-SP 296), 789
Urry, C. M., Mushotzky, R. F., & Holt, S. S. 1986, ApJ, 305, 369
Urry, C. M., & Padovani, P. 1995, PASP, 107, 803
Voges, W. 1993, Adv. Space Res., 13, 391
von Montigny, C., et al. 1995, ApJ, 440, 525
Wagner, S., et al. 1996, A&A, submitted
White, N. E., Giommi, P., & Angelini, L. 1994, BAAS, 26, 1372
Witzel, A., Wagner, S., Wegner, R., Steffen, W., & Krichbaum, T. 1993, in Sub-arcsecond Radio Astronomy, ed. R. J. Davis & R. S. Booth (Cambridge: Cambridge Univ. Press), 159
Wolter, A., et al. 1996, MNRAS, submitted
Worrall, D. M. 1989, in AGN and the X-Ray Background, ed. N. E. White (ESA-SP 296), 719
Worrall, D. M., Birkinshaw, M., & Gwinn, C. R. 1993, in Sub-arcsecond Radio Astronomy, ed. R. J. Davis & R. S. Booth (Cambridge: Cambridge Univ. Press), 303
Worrall, D. M., & Wilkes, B. J. 1990, ApJ, 360, 396
Wurtz, R., Ellingson, E., Stocke, J. T., & Yee, H. K. C. 1993, AJ, 106, 869